AN ABSTRACT OF THE THESIS OF

Adam K. Carlton for the degree of Master of Science in Civil Engineering presented on June 22, 2007.
Title: Finite Element Modeling of Reinforced Concrete Bridge Columns with Steel Jackets Using Plastic Hinge Integration

Abstract approved: _____
Michael H. Scott

Abstract: In recent years confinement requirements for concrete columns have increased in seismic regions. Steel jackets are one way to confine reinforced concrete columns. The increased confinement provides additional strength and ductility for the columns during seismic events. For reinforced concrete columns with steel jackets, there are different section properties in the jacketed and non-jacketed regions. The variation can cause difficulties modeling the seismic response of these columns. A plastic hinge integration method, derived from the modified two-point Gauss-Radau quadrature rule, is used to model steel jacketed columns with force-based finite elements. This integration method allows for the specification of the plastic hinge length in the element, thereby confining the spread of material nonlinear response to selected regions. Controlling the location of material nonlinear response provides an objective numerical solution for strain-softening behavior that occurs due to the crushing of concrete. In addition, different material properties can be specified for the jacketed and non-jacketed regions, which allows for only one frame element to be

used in modeling. This integration method is verified for elements with different material properties using a single force-based beam-column element. After the verification, the integration method is validated against experimental data from tests of steel jacketed reinforced concrete bridge columns conducted at the University of California at San Diego. The results of this research will be incorporated in pushover analysis software, developed at Oregon State University, for Alaska-style bridge bents.

Finite Element Modeling of Reinforced Concrete Bridge Columns with Steel Jackets Using Plastic Hinge Integration

by
Adam K. Carlton

A THESIS

submitted to

Oregon State University

in partial fulfillment of
the requirements for the
degree of

Master of Science

Presented June 22, 2007
Commencement June 2008

Master of Science thesis of Adam K. Carlton presented on June 22, 2007.

APPROVED:

Major Professor, representing Civil Engineering

Head of the School of Civil and Construction Engineering

Dean of the Graduate School

I understand that my thesis will become part of the permanent collection of Oregon State University libraries. My signature below authorizes release of my thesis to any reader upon request.

Adam K. Carlton, Author

ACKNOWLEDGMENTS

The author expresses sincere appreciation to Dr. Scott for providing theoretical and analytical assistance.

CONTRIBUTION OF AUTHORS

Dr. Scott contributed with the theoretical and analytical portions of this thesis.

TABLE OF CONTENTS

Page

Finite Element Modeling of Reinforced Concrete Bridge Columns with Steel Jackets Using Plastic Hinge Integration 1

Chapter 1: Introduction 1

Chapter 2: Verification of the Modified Hinge-Radau Integration Method for Force-Based Beam-Column Elements 3

Introduction 3

Force-Based Element Formulation 4

Force-Based Element Integration Methods 6

Example of Non-Objective Response 7

Plastic Hinge Integration 10

Modeling for Cantilever Example 11

Theoretical Solution 13

Modeled Solution for Cantilever Example 17

Results of Cantilever Example 18

Conclusions 19

References 20

Chapter 3: Modeling of Circular Concrete Bridge Columns with Steel Jackets using Force-Based Beam-Column Elements with Modified Hinge-Radau Integration 21

Introduction 21

Background 23

Material Behavior 26

TABLE OF CONTENTS (Continued)

Page

Case 1: Steel Jacket Around Plastic Hinge Region 30

Case 2: Continuous Steel Jacket 34

Case 3: Continuous Steel Jacket in the Elastic Region.....40

Conclusion 45

References.....46

Chapter 4: Conclusions.....48

Bibliography.....49

Appendices.....51

Appendix A: Theoretical Solution for Cantilever.....51

Appendix B: Hand Calculations for Load Capacity for Case 3.....54

LIST OF FIGURES

Figure Page

2.1: Simply supported basic system and element cross section.....6

2.2: Geometry for example of strain softening behavior using Gauss-Lobatto integration. 8

2.3: Load vs. displacement for three-story reinforced concrete structure modeled with 6, 7, and 8 Gauss-Lobatto integration points. 9

2.4: Location of hinge-Radau integration points. 11

2.5: Moment curvature relationship for strain hardening, perfectly plastic, and strain softening behavior.....12

2.6: Geometry of cantilever used in verification.....13

2.7: Curvature distribution for the cantilever beam.....15

2.8: Comparison of results between the hinge-Radau model, the two element Gauss-Lobatto model, and the theoretical response.....18

2.9: Cantilever displacement response for a point load for strain hardening, perfectly plastic, and strain softening behavior.....19

3.1: The three types of columns modeled. 23

3.2: Description of the bond transfer length to develop composite flexural strength; The geometry of the column with the steel jacket (a); the stress distribution for a steel jacket (b); and the stress distribution for a steel jacket with inadequate development length (c).....26

3.3 Stress strain plot for steel material model.....27

3.4: Stress strain plot for concrete material model.....28

3.5: Stress strain plot for prestressing material model.....28

3.6: An example of the OpenSees code for defining a section. 29

3.7: Geometry for case 1.....31

LIST OF FIGURES (Continued)

Figure Page

3.8: Results for test 1 and test 2 for case 1 of a lateral pushover analysis.....34

3.9: Geometry for case 2. 36

3.10: OpenSees model layout for case 2. 37

3.11: Composite circular column section for case 2.....38

3.12: Comparison for case 2 of the experimental results and the modeled results.....40

3.13: Geometry for case 3.....42

3.14: OpenSees model layout for case 3.....43

3.15: Modeled results for case 3 compared to the hand calculations.....45

B.1: Flexural resistance of the concrete section.....55

LIST OF TABLES

Table Page

3.1: Concrete Strength for Case 1.....32

B.1: Calculations for Flexure in a Reinforced Concrete Section.....56

Finite Element Modeling of Reinforced Concrete Bridge Columns with Steel Jackets Using Plastic Hinge Integration

Chapter 1: Introduction

The modeling of inelastic behavior in framing members is necessary for simulating a structural response from severe lateral loadings. Inelastic behavior occurs in the form of plastic hinges, which are modeled with distributed plasticity. The recognition that inelasticity occurs has created a need to consider plastic hinges in design. This has led to increased confinement requirements for the design of reinforced concrete columns (Chai et al. 1994). Steel jackets are used to confine concrete and improve structural performance during a seismic event. For reinforced concrete columns with steel jackets, different section properties can occur in the plastic hinge region and linear-elastic region for two reasons: either the jacket is not continued across the entire column, or the bond development length prevents full composite action between the jacket and the concrete column (Chai et al. 1994). The use of reinforced concrete columns with steel jackets creates a need for an accurate and computationally efficient numerical model which can represent a beam-column with two different section properties and objectively model strain softening behavior that may occur due to crushing of concrete.

Scott and Fenves (2006) propose a plastic hinge integration method based on Gauss-Radau quadrature that is recommended for nonlinear material modeling of frame structures with strain softening. In this thesis, it is proposed that this integration method is ideal to simulate the behavior of reinforced concrete columns with steel jackets. This plastic hinge integration method allows different section properties to be

specified for the plastic hinge region and the elastic region of an element. These capabilities enable structural behavior to be accurately modeled using only one element per frame member.

This thesis is comprised of two manuscripts. The first manuscript discusses the new plastic hinge integration method and verifies that it can be used to model a frame member with different section properties in the plastic hinge region and the linear-elastic region. This is done by modeling a cantilever with different section properties for the plastic hinge region and the linear-elastic region. The second manuscript examines three types of bridge columns with steel jackets subject to lateral loads and discusses the modeling of the column response. The data from experimental testing for these columns comes from Hewes and Priestly (2002) and Silva et al. (1999). The simulated results are then compared to the experimental results.

Chapter 2: Verification of the Modified Hinge-Radau Integration Method for Force-Based Beam-Column Elements

Introduction

To support applications in performance-based earthquake engineering the modeling of distributed plasticity is necessary to evaluate the likelihood of structural failure under extreme loadings. For a nonlinear analysis, it is desirable to use a single finite element to represent each member of a frame structure. Using only one element per frame member decreases the number of equilibrium equations required in the simulation, creating a more computationally efficient model. There are two prominent formulations for modeling frame members. The first approach uses a displacement-based finite element formulation, which utilizes cubic Hermitian polynomials for the transverse displacement; however, difficulties occur because the assumed displacement field is inexact for nonlinear material behavior (Neuenhofer and Filippou 1997). A force-based beam-column approach, instead, derives the beam-column element stiffness through interpolation functions based on the second order differential equations for bending and axial loading, providing an accurate response for nonlinear material behavior (Neuenhofer and Filippou 1997).

Models simulating nonlinear behavior can be either concentrated plasticity or distributed plasticity. Concentrated plasticity beam-column elements lump the nonlinear material behavior at the ends of the element. Concentrated plasticity does not provide an accurate response for axial-moment interaction. Distributed plasticity

beam-column elements allow nonlinear material behavior to spread across an element. Problems can occur with distributed plasticity in force-based elements because of how the governing equations are numerically integrated. Numerical integration can lead to a loss of objectivity if the distribution of the integration points restricts the location of plasticity. This loss of objectivity occurs for perfectly plastic and strain softening behavior. Plastic hinge integration is used in elements to model distributed plasticity without a loss of objectivity. Additionally, the increased use of steel jackets to confine reinforced concrete columns has created a need to model frame members that have different section properties along their lengths. Plastic hinge integration using modified two-point Gauss-Radau quadrature, also referred to as hinge-Radau integration, is ideal to model such members because different section properties can be specified for each region. This chapter verifies that the hinge-Radau integration method can simulate this behavior by modeling a cantilever having two regions with different material section properties.

Force-Based Element Formulation

Force-based beam-column elements are formulated in a two-dimensional, three degree of freedom basic system. Deformations are assumed to remain small compared to the element length. After removing rigid body displacement nodes, the three degrees of freedom possible for each element are rotation at both ends and axial translation at one end as shown in Figure 2.1. The vector $\mathbf{q} = \mathbf{q}(\mathbf{v})$ is the force vector for the basic system, and it is dependent on the element deformations. Rigid body

equilibrium of the basic forces is included to account for all six degrees of freedom in two dimensional analysis. The section deformations are described by the vector **e**, and correspond to the section forces described by **s** = **s(e),** where **s** is a function of the section deformations **e**. The equilibrium between the forces in the basic system and the section forces is described by,

$$\mathbf{s} = \mathbf{b}\,\mathbf{q} \tag{2.1}$$

where **b** is the matrix with the interpolation functions relating the section forces, **s**, and the basic forces **q**. The matrix **b** is

$$\mathbf{b} = \begin{pmatrix} 1 & 0 & 0 \\ 0 & x/L-1 & x/L \end{pmatrix} \tag{2.2}$$

The principle of virtual forces imposes the compatibility condition expressed by

$$\mathbf{v} = \int_0^L \mathbf{b}^T \mathbf{e}\; dx \tag{2.3}$$

$$\mathbf{e} = [\varepsilon(x), \kappa(x)] \tag{2.4}$$

where ε(x) is the axial strain and κ(x) is the curvature.

When linearized with respect to **q**, Equation (2.3) gives the flexibility matrix

$$\mathbf{f} = \frac{\partial \mathbf{v}}{\partial \mathbf{q}} = \int_0^L \mathbf{b}^T \mathbf{f}_s \mathbf{b}\; dx \tag{2.5}$$

where $\mathbf{f}_s = \mathbf{k}_s^{-1}$ is the section flexibility matrix, which is the inverse of the section stiffness $\mathbf{k}_s = \dfrac{\partial \mathbf{s}}{\partial \mathbf{e}}$. The inverse of **f** is the stiffness matrix **k** which is transformed and assembled in the finite element equations. For computer implementation the compatibility relationship from Equation (2.3) is evaluated by numerical integration

$$\mathbf{v} = \sum_{i=1}^{N_P} (\mathbf{b}^T \mathbf{e} \mid_{x=\xi_i}) \omega_i \tag{2.6}$$

where ξ and ω are the locations and associated weights of the integration points. Similarly, the flexibility matrix is determined by

$$\mathbf{f} = \sum_{i=1}^{N_P} (\mathbf{b}^T \mathbf{f}_s \mathbf{b} \mid_{x=\xi_i}) \omega_i \tag{2.7}$$

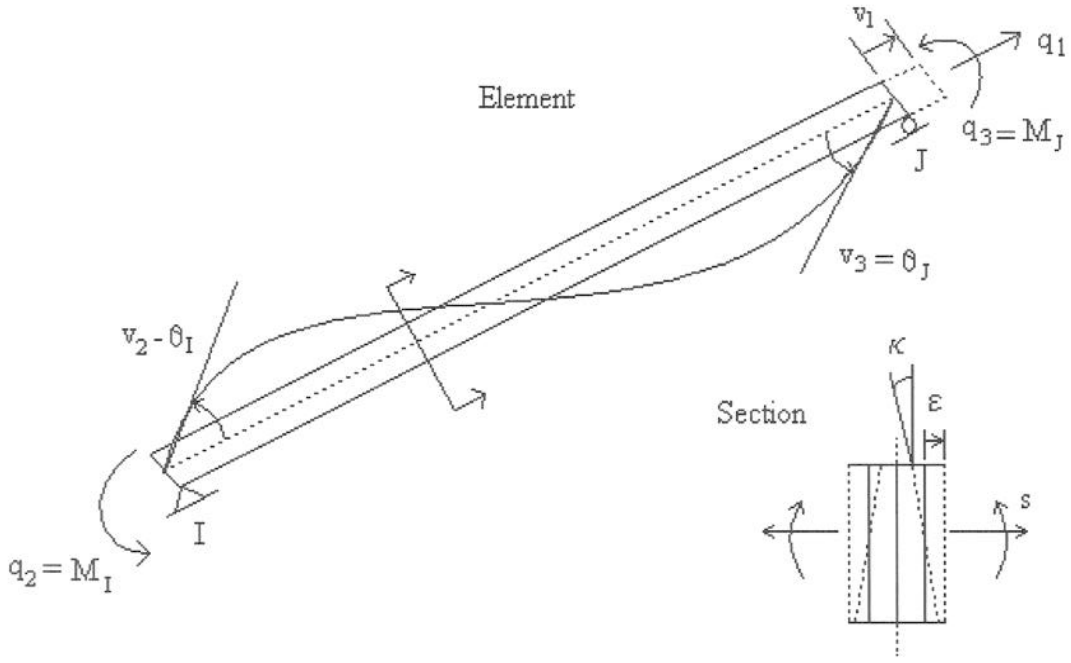

Figure 2.1: Simply supported basic system and element cross section.

Force-Based Element Integration Methods

Gauss-Lobatto integration is commonly used with force-based beam-columns to evaluate Equations 2.6 and 2.7. This numerical integration method uses one integration point at each end with the remainder of the integration points distributed between the two ends according to optimality constraints for the integration of high

order polynomials. This method is commonly used because it samples forces at the end of the columns, where the moments are the largest in the absence of member loads. Gauss-Lobatto integration can exactly model linear-elastic behavior with three integration points and accurately integrates polynomials of up to degree $2N_p$-3 where N_p is equal to the number of integration points used. Gauss-Lobatto integration models strain hardening behavior by allowing plasticity to spread across the element. To get accurate results for strain hardening behavior it is necessary to use at least four or five integration points. While Gauss-Lobatto integration can model strain hardening behavior, strain softening and perfectly plastic behavior create computational problems because plasticity is confined to the first integration weight regardless of the number of integration points used. This causes the plastic hinge length to be dependent on the number of integration points specified by the analyst instead of the length observed in the field or predicted by empirical relationships. The result is a loss of objectivity in the computed response for strain softening and perfect plasticity when using Gauss-Lobatto integration because the response changes as a function of the number of integration points.

Example of Non-Objective Response

To show the loss of objectivity a three story frame is modeled using six, seven, and eight point Gauss-Lobatto integration. The geometry and details are shown in Figure 2.2. The beams and columns are spaced at 4 m on center. The columns are 300 mm by 300 mm and the beams are 150 mm by 300 mm. The columns have four M29

bars and the columns have four M25 bars. Strain softening occurs in the members due to crushing in the concrete.

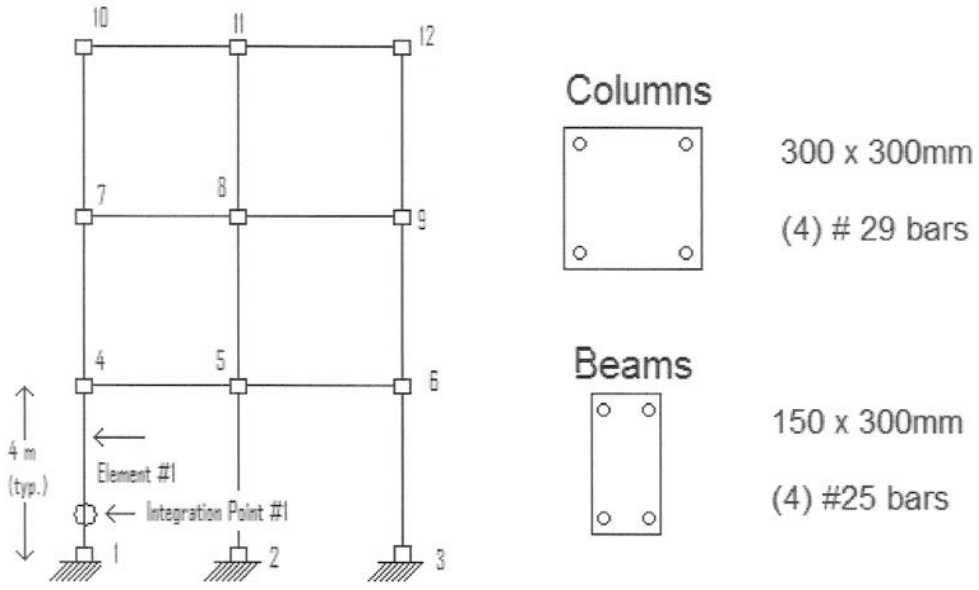

Figure 2.2: Geometry for example of strain softening behavior using Gauss-Lobatto integration.

This frame structure is modeled and subjected to a incremental lateral displacement of node 11. The results from the pushover analysis are shown in Figure 2.3 where the post-peak structural response varies depending on the number of integration points used to model each element. The variation in the response occurs because the plastic hinge is being defined differently in each case. As the plastic hinge length becomes smaller, less force is required to maintain equilibrium for a given displacement. For an objective solution, the post yield behavior should not be dependent on the number of integration points used.

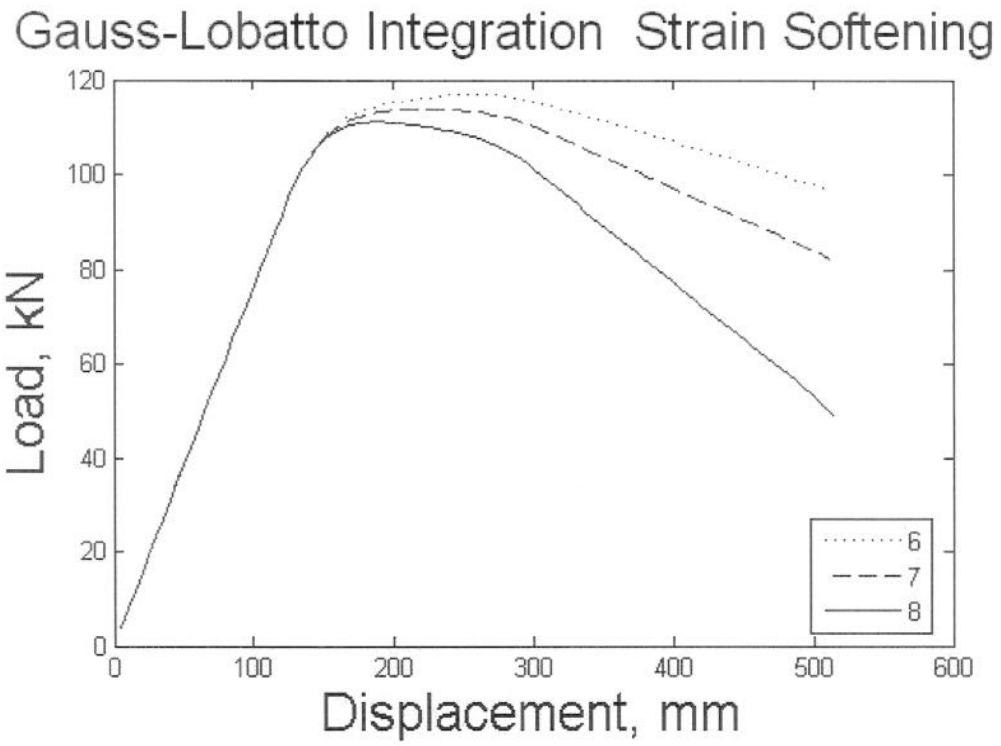

Figure 2.3: Load vs. displacement for three-story reinforced concrete structure modeled with 6, 7, and 8 Gauss-Lobatto integration points.

To correct the loss of objectivity, Coleman and Spacone (2001) provide a regularization technique to maintain the objectivity of the localized response using the constant fracture energy criterion. This allows for any number of integration points to be used and still provide an objective element response. However, to regularize the solution it is necessary to modify the material properties, creating a loss of objectivity in the material response. Another approach is hinge-Radau integration, which instead of modifying the material properties to change the localized curvature, allows the analyst to fix the length of the plastic hinge to provide an objective response at the element and material levels (Scott and Fenves 2006).

Plastic Hinge Integration

The hinge-Radau integration method maps two-point Gauss-Radau quadrature on to the lengths $4(L_p)_i$ and $4(L_p)_j$ at the ends of an element, where L_p is the plastic hinge length. Two-point Gauss-Radau quadrature over [0,1] has integration points at 0 and 2/3 with integration weights of 1/4 and 3/4 respectively. The first integration point is located at one of the ends of the element, and it has an integration weight equal to L_p. The second integration point is located $8/3L_p$ into the element and has an integration weight of $3L_p$. The other two integration points are symmetrically located on the opposite end of the element. The portion of the element that is not within four plastic hinge lengths from either end is modeled as linear-elastic because the plastic hinge assumption is that inelasticity is confined to the plastic hinge regions. The location of the integration points is shown in Figure 2.4. This integration method allows for the section force-deformation relationship to be evaluated at the end of the element where the bending moment is largest in the absence of distributed loads. The two point method allows for exact integration of quadratic polynomials across hinges giving an exact theoretical solution for linear-elastic prismatic elements. The plastic hinge region is modeled with one integration weight to maintain objectivity because the weight is defined by the analyst as the plastic hinge length. Another benefit of this integration method is that the analyst can specify different section properties for the plastic hinge regions and the elastic region to accommodate elements with different material properties along their length.

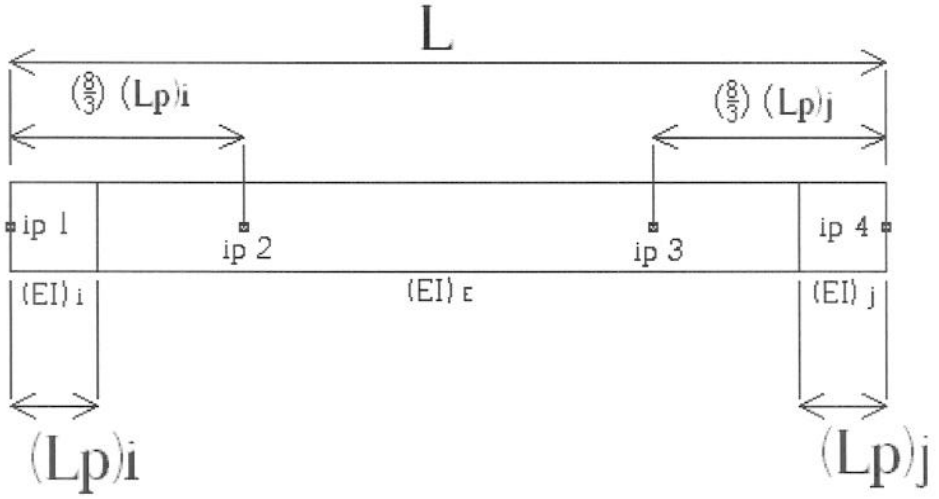

Figure 2.4: Location of hinge-Radau integration points.

Modeling for Cantilever Example

The accuracy of the hinge-Radau integration method for beam columns with differing flexural stiffness (EI) between the plastic hinge region and the elastic region is verified by computing a theoretical solution and comparing it to a solution modeled using hinge-Radau integration. To verify the theoretical solution, an approximate solution is modeled using two force-based elements that is compared to the other two solutions. The finite element models were constructed using the Open System for Earthquake Engineering Simulation (OpenSees) (McKenna et al. 2000). OpenSees is an object oriented framework for finite element analysis, using the Tcl/Tk programming language. It is open source software intended for use in the research community, and it provides an ideal environment to test different integration options.

Three cases of post yield behavior are modeled using hinge-Radau integration. The first is strain hardening, the second is perfect plasticity, and the third is strain softening. Strain softening occurs when increased curvature takes place with a

decrease in moment. An example of strain softening is crushing in concrete. These three cases are modeled to show that objective solutions are found for perfectly plastic and strain softening behavior. For the three cases, the inelastic responses are modeled by defining a variable $\alpha(\mathrm{EI})$. Where α is the percentage of the original stiffness which represents the post yield response. The variable α is equal to 0.02 for strain hardening, zero for perfect plasticity, and -0.02 for strain softening. For these cases the post yield responses are linear and are shown in Figure 2.5. These linear post yield responses are simplified versions of real material behavior. Fiber discretized cross-sections can be used to more accurately model the beam's response. An example of a more complicated section response is presented in the second chapter.

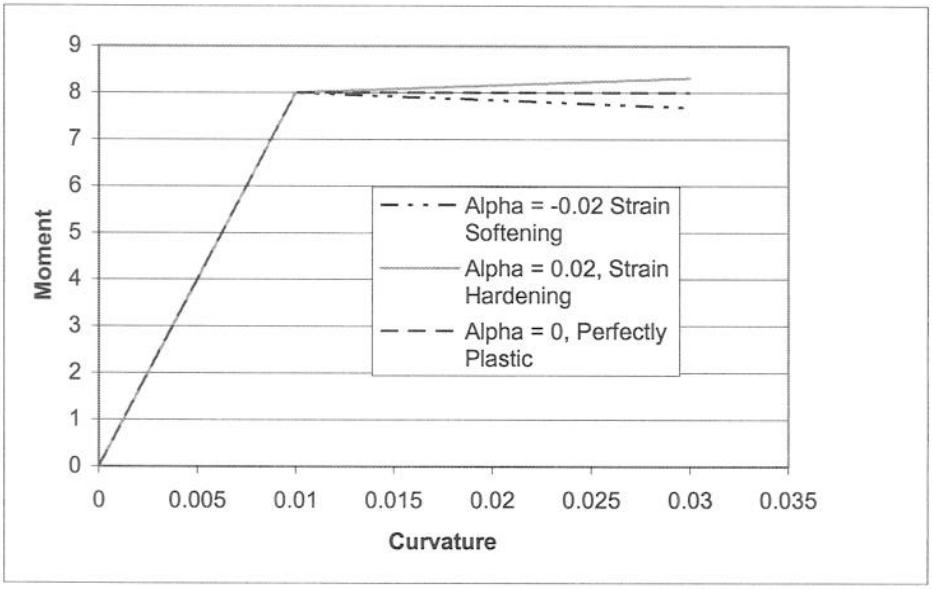

Figure 2.5: Moment curvature relationship for strain hardening, perfectly plastic, and strain softening behavior.

Theoretical Solution

The theoretical solution corresponds to the force-displacement response of a cantilever with a transverse load P applied at the free end. The cantilever has a plastic hinge length of $(L_p)_i$. A theoretical solution exists only for strain hardening behavior while the other two types of behavior lead to singularities in the theoretical solution. The displacement is measured from the free end of the cantilever shown in Figure 2.6.

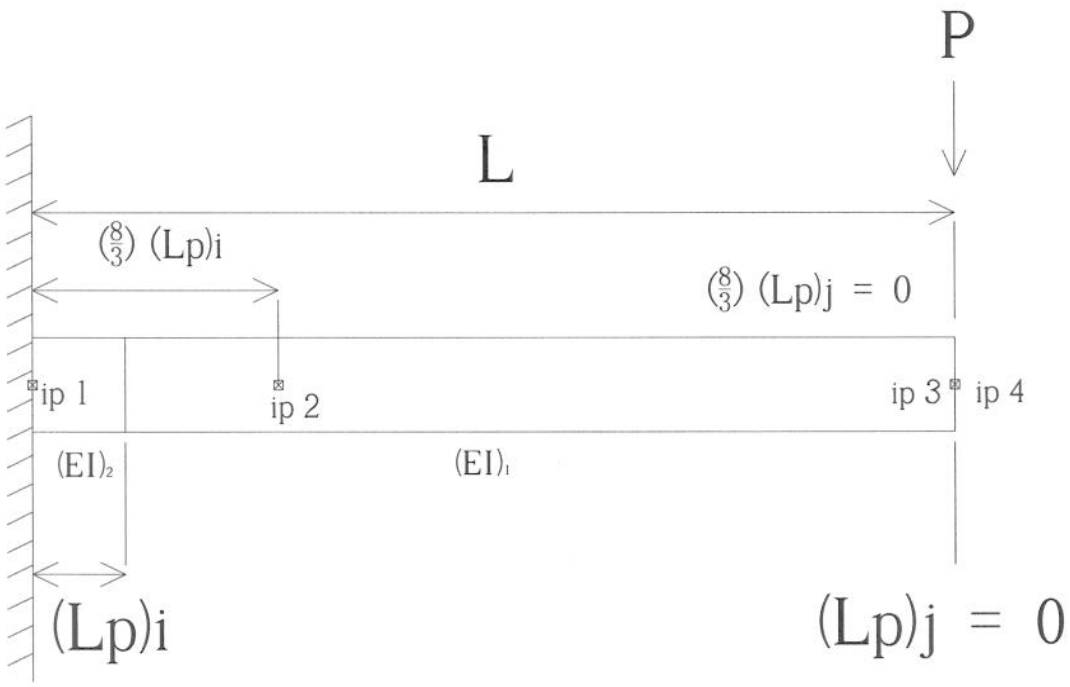

Figure 2.6: Geometry of cantilever used in verification.

The beam has a constant cross section and a stiffness of $(EI)_1$ in the elastic region and stiffness $(EI)_2$ in the plastic hinge region. The moment-curvature response is bilinear with a yield moment M_y and a hardening ratio α. The theoretical response

for the displacement of the beam is shown in Equations 2.7 and 2.8. For the derivation of these equations see Appendix A. The variable β is defined as $\beta = L_p/L$. The variable ζ is defined as the length from the fixed end of the cantilever to where M is greater than M_y in the cantilever. It represents the length of the beam undergoing an inelastic response.

For $P < P_y$ use

$$U = P\frac{(L-\beta L)^3}{3E_1I_1} + P\frac{[(L)^3-(L-\beta L)^3]}{3E_2I_2} \tag{2.7}$$

And for $P > P_y$ use

$$U = U_1 + U_2 + U_3 + U_4 \tag{2.8}$$

where:

$$U_1 = P\frac{(L-\beta L)^3}{3E_1I_1} \tag{2.9}$$

$$U_2 = P\frac{[(L-\zeta L)^3-(L-\beta L)^3]}{3E_2I_2} \tag{2.10}$$

$$U_3 = M_y\left(\frac{L^3-(L-\zeta L)^3}{3E_2I_2}\right) \tag{2.11}$$

$$U_4 = \left(\frac{PL^3[(4\zeta-1)+(1-\zeta)^4]}{12\alpha E_2I_2}\right) \tag{2.12}$$

$$\zeta = \max(0, 1 - My / M)$$

$$\beta = L_p / L$$

These equations describe the displacement of the free end of the cantilever beam with an applied load P. Equation 2.7 describes the behavior prior to yield and Equation 2.8 describes the response after yield has occurred. When looking at the behavior of the beam the four terms of this equation describe separate parts of the beam's behavior.

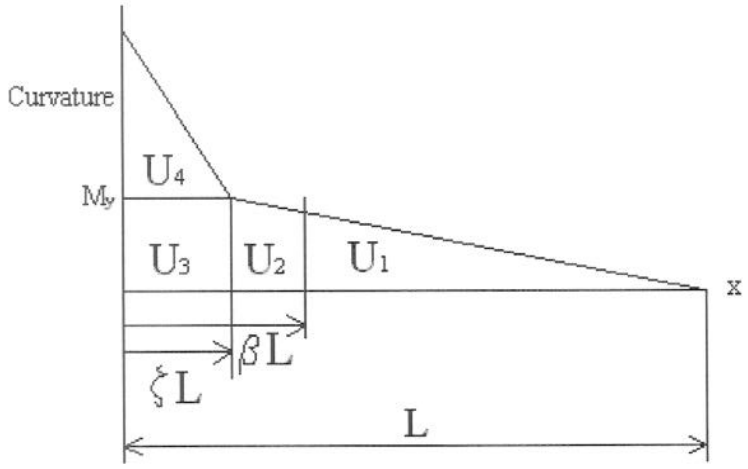

Figure 2.7: Curvature distribution for the cantilever beam.

1) The first term (U_1) describes displacement due to the elastic region. This region continues to deform elastically when the plastic hinge region deforms inelastically.

2) The second term (U_2) is the elastic portion of the deformation of the plastic hinge region. The area over which this section occurs is controlled by ζ in the equation. Prior to yield at the end of the beam ζ is equal to zero. After yield has spread across the whole region, ζ is equal to β causing the term to go to zero.

3) The third term (U_3) in the equation is the elastic deformation of the plastic hinge region after it has yielded. It remains constant for the entire post yield response and gradually spreads across the plastic hinge region until it covers the entire region. The length of this region is also controlled by ζ. It starts at the fixed end and is of length ζ L. The sum of the lengths over which U_2 and U_3 apply is always equal to βL, which is the length of the plastic hinge.

4) The fourth term (U_4) describes the inelastic behavior of the plastic hinge section. This term is defined from the fixed end and is ζL in length. It is the length of the beam that is in an inelastic response. The inelastic behavior is always confined to the plastic hinge region βL from the fixed end.

Modeled Solution for Cantilever Example

The model built in OpenSees is a one member cantilever beam. It consists of two nodes and one force-based beam-column element with hinge-Radau integration. It is made in a two dimensional, three degree of freedom system. Node one is fixed in all directions and node two is unrestrained. The location of the integration points can be seen in Figure 2.6. The cantilever has a unitless length of ten and a plastic hinge length of one. The section properties for the element are linear-elastic to yield point and then there is either strain hardening at 2% of EI, perfect plasticity, or strain softening at -2% of EI. The stiffness, EI, for this model is 800 and 600 for the plastic hinge region and the elastic region, respectively. The yield moment is eight for the whole beam. A plot of the moment-curvature relationship in the plastic hinge region is shown for each type of post yield response in Figure 2.5. The model uses a displacement controlled integrator to calculate the load because in the strain softening case the load decreases after the yield point. Load controlled integration fails at yield for strain softening because the increased load step would not converge to equilibrium.

The theoretical solution is verified by an OpenSees solution using two elements. The plastic hinge region is modeled by the first element, and it is a force-based element with ten-point Gauss-Lobatto. The large numbers of integration points approximate a closed form solution, and allow the plasticity to spread freely through the element. The second element models the elastic region and it is a force-based element with three-point Gauss-Lobatto integration that remains linear-elastic. This

solution is only modeled for strain hardening because perfectly plastic and strain softening behavior do not give an objective response.

Results of Cantilever Example

From the comparison of the force displacement plot in Figure 2.8, it is seen that hinge-Radau integration provides a similar solution to the theoretical solution for strain hardening. All of the solutions show that the cantilever beam remains linear-elastic up to the yield point. After yield the hinge-Radau solution is more flexible than the other solutions because it does not take into account the gradual spreading of plasticity across the plastic hinge. The results for all three cases using hinge-Radau integration are shown in Figure 2.9, where an objective response is achieved for all three cases.

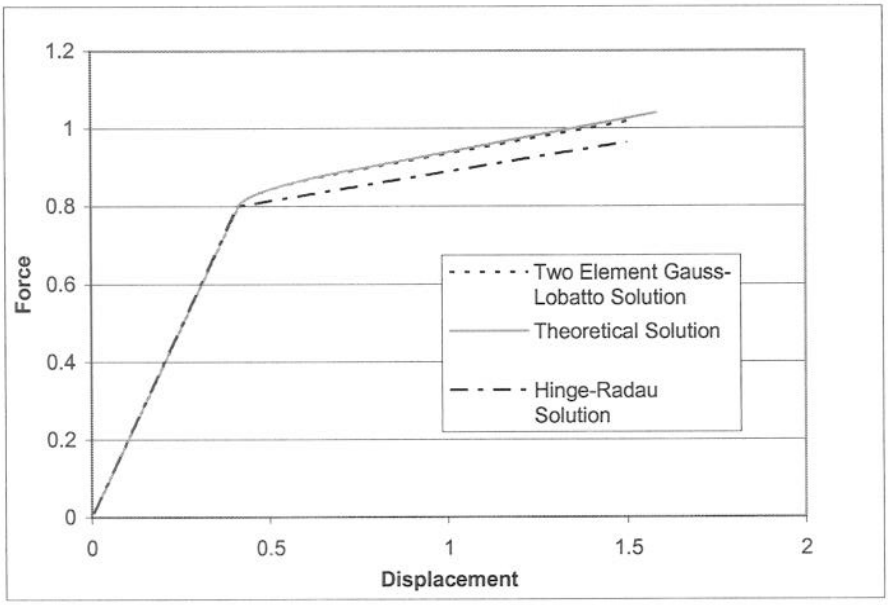

Figure 2.8: Comparison of results between the hinge-Radau model, the two element Gauss-Lobatto model, and the theoretical response.

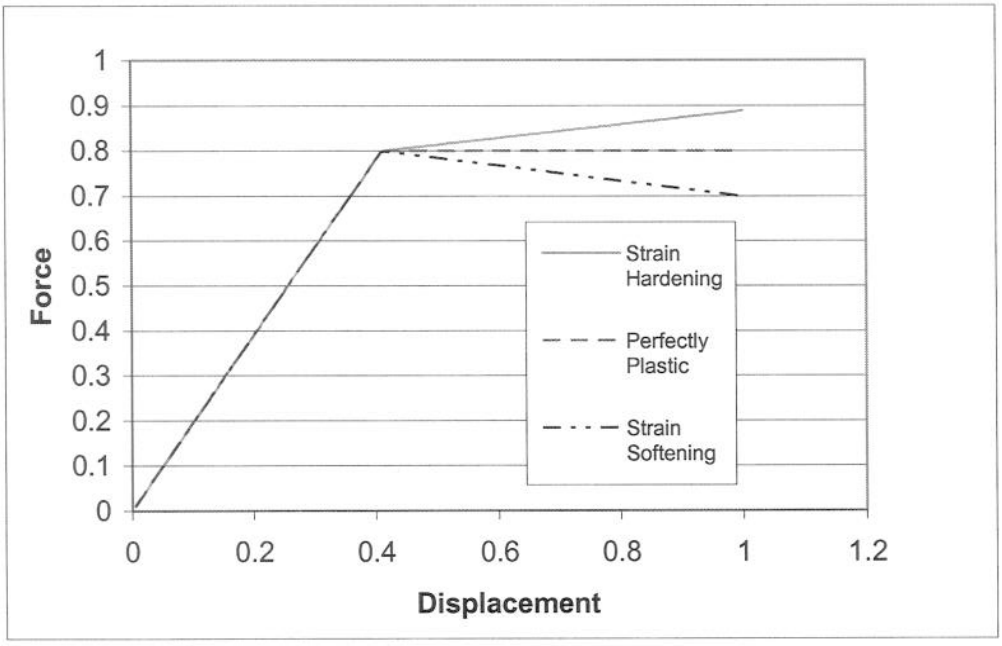

Figure 2.9: Cantilever displacement response for a point load for strain hardening, perfectly plastic, and strain softening behavior.

Conclusions

This chapter compares the post-yield response of a cantilever modeled using hinge-Radau integration and the computed theoretical response for a cantilever beam with a transverse load applied at the free end. The hinge-Radau integration method uses a minimum number of integration points and elements to compute an approximate solution for a cantilever with a nonlinear response distributed across the plastic hinge region. The comparison shows that the numerical solution using hinge-Radau integration closely matches the theoretical solution. This verifies that the hinge-Radau integration method can be used to model the behavior of more complicated

structural systems with beam-columns that have plastic hinges, and make the solution method as efficient as possible.

References

Coleman, J. and Spacone, E. (2001). "Localization issues in force-based frame elements." *Journal of Structural Engineering*, Vol. 127, No. 11, 1257-1265.

McKenna, F., Fenves, G. L., Scott, M. H., and Jeremic, B. (2000). "Open system for earthquake engineering simulation" <http://opensees.berkeley.edu>

Neuenhofer, A., and Filippou, F. C. (1997). "Evaluation of nonlinear frame finite-element models." *Journal of Structural Engineering*, 123(7), 627-641.

Neuenhofer, A., and Filippou, F. C. (1998). "Geometrically nonlinear flexibility-based frame finite element." *Journal of Structural Engineering*, 124(6), 704-711.

Scott, M. H., and Fenves, G. L. (2006). "Plastic hinge integration methods for force-based beam–column elements." *Journal of Structural Engineering*, 132(2), 244-252.

Spacone, E., Ciampi,V., and Filippou, F. C. (1996). "Mixed formulation of nonlinear beam finite element." *Computers & Structures*, 58,71-83.

Chapter 3: Modeling of Circular Concrete Bridge Columns with Steel Jackets using Force-Based Beam-Column Elements with Modified Hinge-Radau Integration

Introduction

In seismic regions bridge design using reinforced concrete columns is common place. After the 1971 San Fernando Earthquake the confinement requirements for column design were increased. The confining ratios of the columns designed prior to 1971 are approximately less than one-fifth the current design requirements (Chai et al. 1994). Steel jackets have been used to add confinement to deficient columns. Confinement, either with steel jackets or spiral reinforcement, increases concrete strength and ductility. The use of steel jackets to improve the performance of new and retrofitted structures is gaining popularity because steel jackets easily attach to columns.

The increased use of steel jackets to add confinement to bridge columns has created a need for finite element modeling of these structures. Two common approaches to modeling frame members are displacement-based and force-based element formulations. The displacement-based formulation utilizes cubic Hermitian polynomials for the transverse displacement, which results in linear curvature for the element. This provides exact results for linear-elastic beam columns, but difficulties occur with nonlinear analysis (Neuenhofer and Filippou 1997). Force-based elements are formulated using interpolation functions for the internal forces of the element, which are based on second order differential equations for bending and axial loading. Force-based elements provide an accurate response for nonlinear behavior.

This chapter examines the modeling techniques of steel jacketed circular concrete columns with force-based beam-column elements using hinge-Radau integration. Scott and Fenves (2006) used hinge-Radau integration to overcome difficulties that arise with Gauss-Lobatto integration for strain-softening behavior in force-based beam-column elements. In addition to modeling strain-softening behavior, hinge-Radau integration can allow the specification of different section properties for the plastic hinge and the elastic regions. The formulation for the force-based beam-column elements with hinge-Radau integration and the verification for specifying different section properties for the linear-elastic and the plastic hinge section are discussed in the previous chapter.

Three cases of reinforced concrete columns with steel jackets are modeled, shown in Figure 3.1. The first case is a concrete column with a steel jacket around the plastic hinge region. This case is modeled based on an experiment conducted at the University of California at San Diego. The experimental data and column design are taken from Hewes and Priestly (2002). The second case is a bent cap with three CISS (cast in-place steel shell) columns with the steel jackets around the entire column, which is based on another experiment conducted at the University of California at San Diego. The experimental data and column design are taken from Silva et al. (1999). The third case is a bent cap with three CISS columns with steel jackets around the elastic region and spirally confined reinforced concrete in the plastic hinge region. The general column geometry and design are taken from Silva et al. (1999). The only modification of the column design is the change to the length of the steel jacket, where

instead of the steel jacket covering the length of the column, the plastic hinge section is exposed with only spirally confined concrete.

OpenSees (Open System for Earthquake Engineering Simulation) (McKenna et al. 2000) is used to model the columns. OpenSees is an object oriented framework for finite element analysis, using the Tcl/Tk programming language. It is open source software intended for use in the research community, and provides an ideal environment to use different integration methods to model reinforced concrete columns with steel jackets.

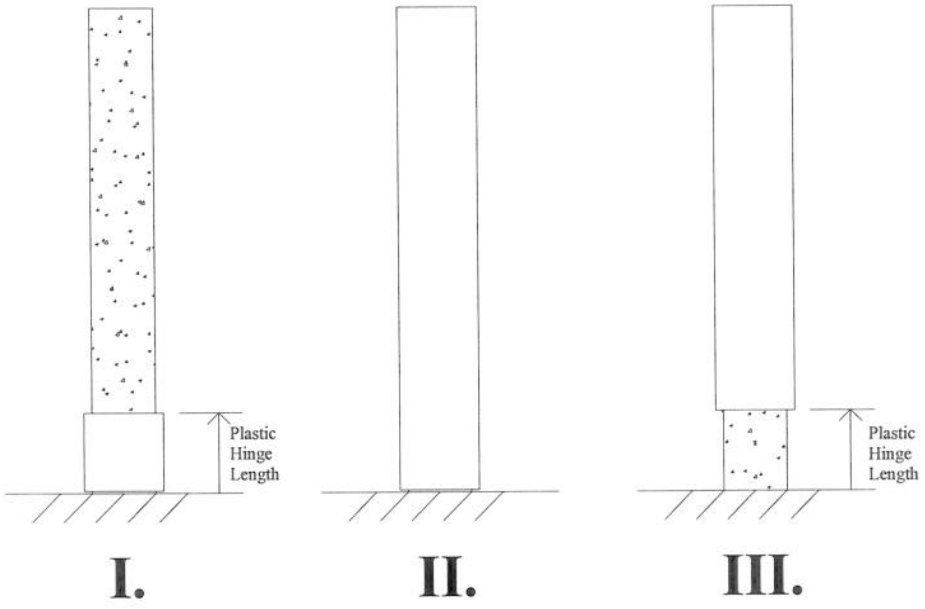

Figure 3.1: The three types of columns modeled.

Background

Steel jackets are used to provide confinement for the concrete. They are added to columns by welding two prefabricated steel shells around a column. The space between the concrete and the steel jacket is grouted to allow composite action between the two materials. The steel jackets must be terminated prior to cap beams and foundations to prevent the jacket from deforming and bearing on the cap beam or foundation. To model the behavior of concrete columns confined by a steel jacket it is necessary to determine the confined strength of the concrete and the bond development length between the concrete and the jacket.

The confined strength of the concrete is calculated using Mander's theoretical stress-strain relationship (Mander et al. 1988).

$$f'_{cc} = f'_{co}\left(-1.254 + 2.254\sqrt{1 + 7.94\frac{f'_l}{f'_{co}}} - \frac{2f'_l}{f'_{co}}\right) \qquad (3.1)$$

Where: f'_{co} = initial concrete strength

$$f'_l = 2f_{yj} * \frac{t_j}{D_j}$$

f_{yj} = yield stress of the steel jacket

t_j = jacket thickness

D_j = jacket diameter

From experimental testing, Chai et al. (1991) has shown that the steel jacket does not need to extend the entire length of the column to provide the desired confinement across the plastic hinge. In practice, the steel jacket frequently extends

the entire length of the column to maintain uniformity. However, in order to obtain flexural strength from the steel jacket it is necessary to account for the transfer length between the concrete and the steel jacket.

To correctly model the steel jacket properties in a section, it is important to account for composite action between the steel jacket and the concrete. The composite action is controlled by the bond strength of the grout used between the jacket and the concrete. Assuming the column is at full composite strength along the length of the steel jacket, there will be a linear stress distribution in the jacket due to the moment caused by the lateral loading. If bond transfer lengths are taken into account, then the stress distribution starts at zero at either end of the steel jacket and approach full composite stress after the transfer lengths. Chai et al. (1994) have proposed a linear relationship through the transfer length, shown in Figure 3.2, with the transfer lengths calculated by

$$l_t = \frac{(L - v_g - L_j)t_j}{[\mu_o L - (f_{vj})_{ave} t_j]} (f_{vj})_{ave} \tag{3.2}$$

$$l_b = \frac{(L - v_g)t_j}{[\mu_o L + (f_{vj})_{ave} t_j]} (f_{vj})_{ave} \tag{3.3}$$

Where

L = Length of the Column

L_j = Length of the Jacket

μ_o = Bond Stress

t_j = Thickness of the Steel Jacket

v_g = Length of the Gap

$(f_{vj})_{ave}$ = Full Composite Strength

It is important to check that $l_b + l_t$ is less than the length of the steel jacket. Otherwise, the stresses never equal the full composite stresses, and have the profile shown in Figure 3.2 (c).

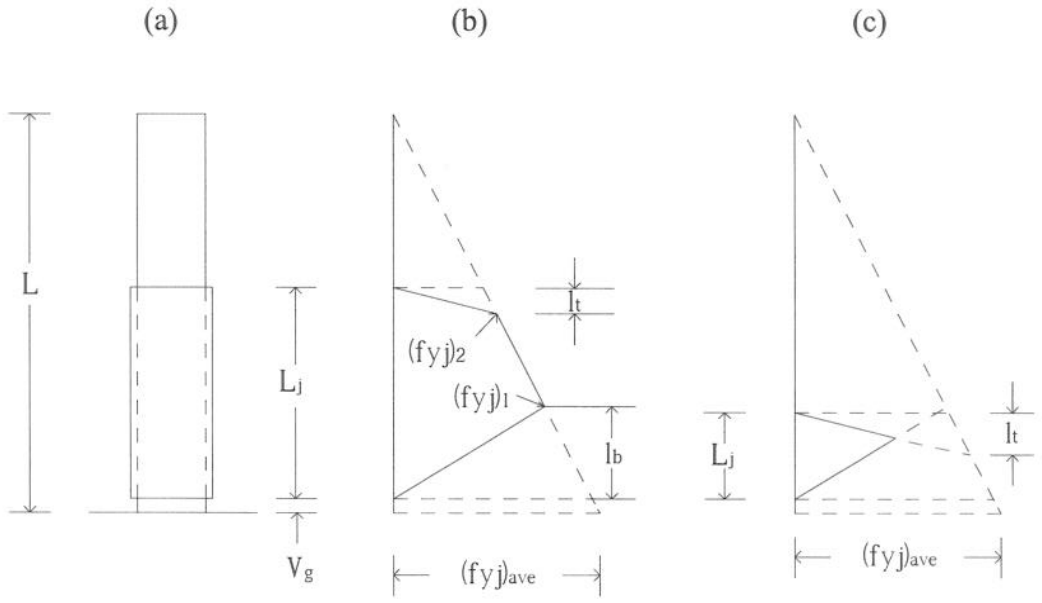

Figure 3.2: Description of the bond transfer length to develop composite flexural strength; The geometry of the column with the steel jacket (a); the stress distribution for a steel jacket (b); and the stress distribution for a steel jacket with inadequate development length (c).

Material Behavior

The material behavior is defined by uniaxial material models available in OpenSees. Steel is modeled using the Steel01 material, which is linear-elastic up to the yield stress. After the steel strength reaches yield, it strain hardens at a percentage, α, of the modulus of elasticity, as is shown in Figure 3.3. Concrete is modeled using the Concrete01 material. The concrete has zero tensile strength, and the compressive

strength is modeled by a parabola starting with a slope 2 f'_c/ε_{co} at zero strain. Then the concrete strength curves to the peak crushing strength, f'_c, at crushing strain, ε_{co}. From the yield point the strength declines linearly to ultimate strength, f'_{cu}, at ultimate strain, ε_{cu}. The material properties of concrete can be seen in Figure 3.4. The prestressing strands, modeled with the PresstressedSteel material, are defined as linear-elastic until yield and then as nonlinear defined by Equation 3.4 (PCI 2004).

$$f_{ps} = f_{ult} - \frac{f_{ult} 1.48 * 10^{-4}}{\varepsilon_{ps} - 0.007} \quad \text{(MPa)} \qquad \text{(Equation 3.4)}$$

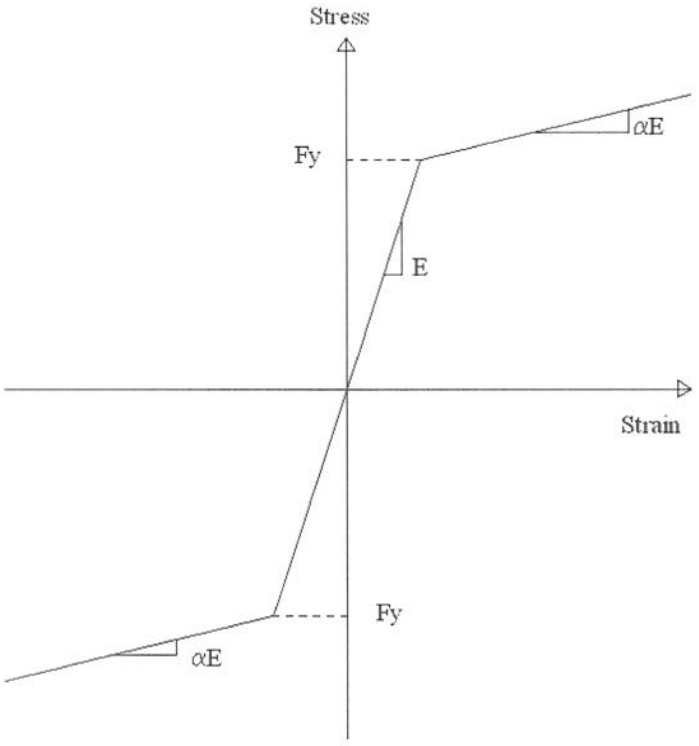

Figure 3.3 Stress strain plot for steel material model.

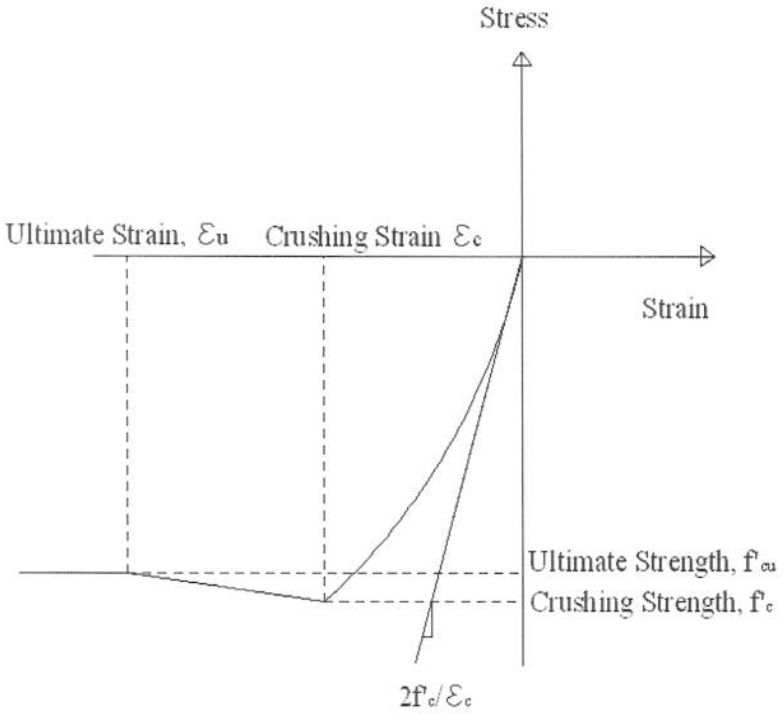

Figure 3.4: Stress strain plot for concrete material model.

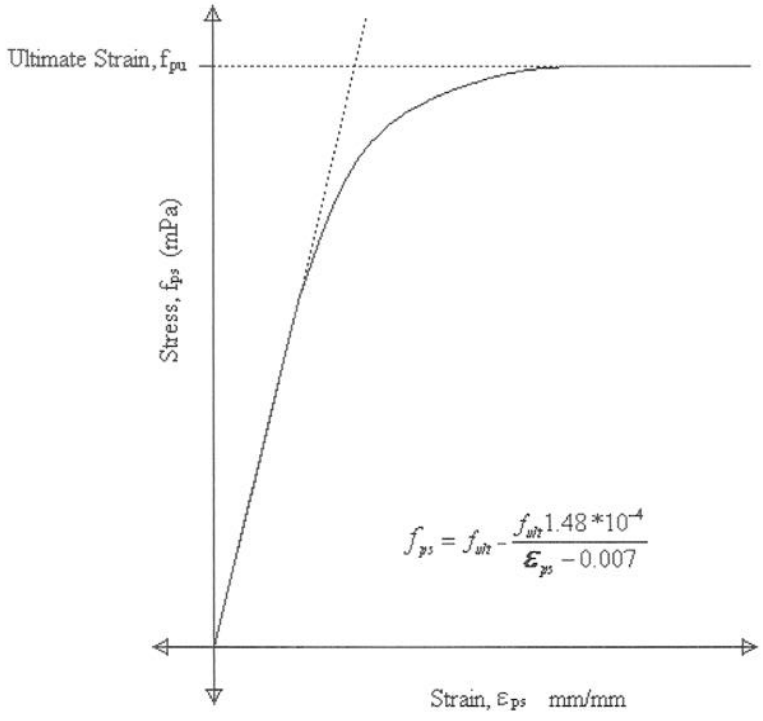

Figure 3.5: Stress strain plot for prestressing material model.

A circular fiber discretization describes the section behavior for all three cases. The circular fiber section combines multiple material properties into one section to more accurately represent the section response and to account for axial-moment interaction. A circular patch command is used in OpenSees for the concrete and the steel shell. The rebar is defined by a circular layer command specifying the number of bars, area of the bars and location of the bars. An example of the OpenSees code describing the sections used in case one is shown in Figure 3.6. The specific section properties are discussed for each case in the following sections.

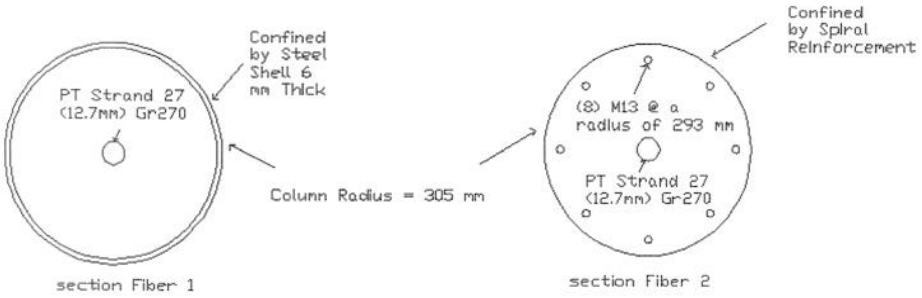


```
section Fiber 1 {

# Concrete
#patch circ $matTag $numSubdivCirc $numSubdivRad $ycenter $zCenter $intRad $extRad
 patch circ $matTag $numSubdivCirc $numSubdivRad $ycenter $zCenter $intRad $interface 0 360

#Strand
#patch circ $matTag $numSubdivCirc $numSubdivRad $ycenter $zCenter $intRad $extRad
 patch circ $matTagpre $numSubdivCircpre $numSubdivRadpre $ycenter $zCenter $intRadpre $extRadpre 0 360

}

section Fiber 2 {

# Concrete
#patch circ $matTag $numSubdivCirc $numSubdivRad $ycenter $zCenter $intRad $extRad
 patch circ 5 $numSubdivCirc $numSubdivRad $ycenter $zCenter $intRad $interface 0 360

#Reinforcing Steel
#layer circ $matTag $numBar $areaBar $yCenter $zCenter $radius
 layer circ $matTagst $numBar $areaBar $yCenter $zCenter $radius

#Prestressing Strand
#patch circ $matTag $numSubdivCirc $numSubdivRad $ycenter $zCenter $intRad $extRad
patch circ $matTagpre $numSubdivCircpre $numSubdivRadpre $ycenter $zCenter $intRadpre $extRadpre 0 360

}
```

Figure 3.6: An example of the OpenSees code for defining a section.

Case 1: Steel Jacket Around Plastic Hinge Region

The first case considered is a circular concrete column with a steel shell around the plastic hinge region. The data used to model the column comes from a report by Hewes and Priestly (2002), which examines the performance of unbonded post-tensioned precast segmental bridge columns under lateral loading during testing conducted at the University of California at San Diego. The displacement in the precast columns is not due to a plastic hinge formation; rather it is caused by a crack formed at the base about which the column rotates as a rigid body. This failure occurs because of the use of precast segments and the steel jacket (Hewes and Priestly 2002). Due to the short length of the steel jacket, the necessary bond length is not developed for composite action. So, the flexural strength of the steel shell is neglected, but confinement from the steel shell is still considered in the concrete stress-strain response.

Geometry for Case 1

Two of the columns from the test done by Hewes and Priestly (2002) have been modeled in this thesis. Both columns have the same geometry and are shown in Figure 3.7. One column was tested at a later date than the other column, allowing the concrete in that column to gain more strength. Both precast columns sit on a 1675 mm by 1675 mm square footing that is 914 mm tall. The columns consist of four precast segments. The bottom segment is 610 mm tall and the other three segments are 914 mm tall; all of the segments are 610 mm in diameter. There are two sections in each

column. One has a steel jacket, and the other does not. The steel jacket attaches around the bottom segment of each column and is also 610 mm tall. The jacket terminates 21mm above the footing to prevent bearing on the foundation. The precast segments have (27) 12.7 mm diameter, grade 270 m, low-relaxation, prestressing strands with a total cross-sectional area of 2665 mm^2. The prestressing strands act through the center of the column. The strands are initially stressed to 40% of ultimate strength for the first test, and 60% of ultimate strength for the second test. Additional mild steel of eight M13 bars (#4) are provided for crack control except in the steel jacket segment.

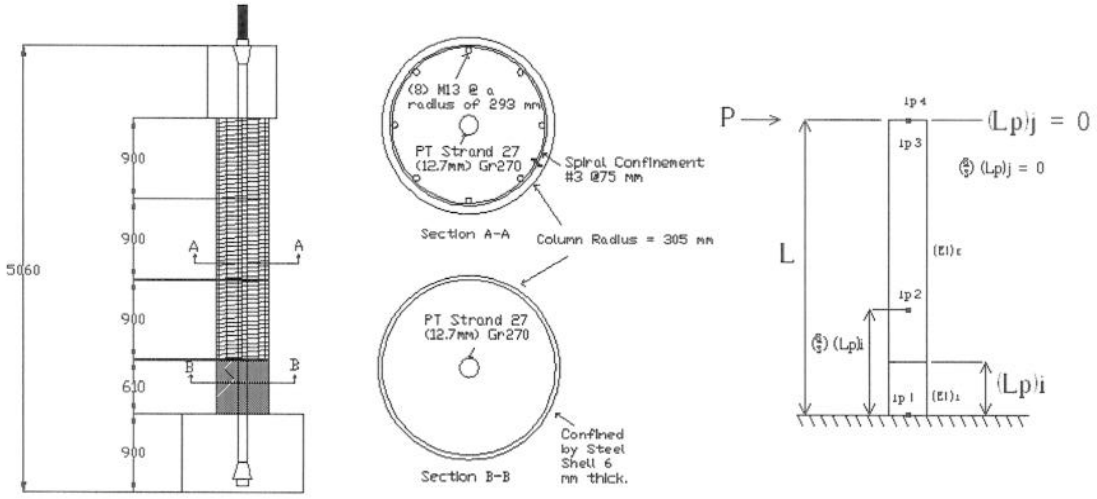

Figure 3.7: Geometry for case 1.

Modeling for Case 1

Case 1 is modeled in a two dimensional system with three degrees of freedom. The model consists of two nodes and one element. The bottom node is fixed

transversely in the X, Y directions and rotationally in the Z direction to simulate a rigid connection. The top node is unrestrained.

A force-based beam-column element with hinge-Radau integration is used. The plastic hinge length is 610 mm for the fixed end, which corresponds to the length of the steel shell. A plastic hinge does not form at the free end where there is no bending moment. Two different sections have been created, one in the plastic hinge region with a steel shell and another in the elastic region without a steel shell.

The material behavior is defined by material models available in OpenSees, as discussed earlier. The reinforcing steel has an elastic modulus of 200,000 MPa and yield strength of 443 MPa with a strain hardening ratio of 2%. The confined concrete strength is determined using Mander et al. (1988), which gives values for f'_c and f'_{cu} at their respective strains. These values depend on the thickness of the steel jacket and the concrete properties. The f'_c and f'_{cu} values are shown in Table 3.1. The steel shell has an elastic modulus of 200,000 MPa with yield strength of 250 MPa. The flexural capacity of the steel jacket is negligible because the transfer lengths overlap. Also the crack between the steel shell and the foundation indicates the steel shell only provides confinement for the concrete (Hews and Priestly 2002). The strands have an ultimate stress of 1,953 MPa

Table 3.1: Concrete Strength for Case 1

	Spirally Confined		Steel Jacket	
	f'_c	f'_{cu}	f'_c	f'_{cu}
Test 1	58 MPa	48.7 MPa	82 MPa	48.7 MPa
Test 2	66 MPa	57 MPa	91 MPa	57 MPa

The section used in the plastic hinge region is a circular composite section combining the concrete, the prestressing strand, and the shell steel. The concrete has a diameter of 610 mm and is confined by the steel jacket. The (27) Grade 270 strands with a gross area of 2665 mm^2 are lumped together into one circular patch. The prestressing strands are jacked to 40% of ultimate strength after losses for the first test and 60% for the second test. This section is shown in Figure 3.7, Section B-B.

The section in the elastic region is a circular composite section combining concrete, prestressing strand, and reinforcing steel. The diameter of the concrete is 610 mm, and it is spirally confined. The prestressing strand is identical to that of the plastic hinge region. The reinforcing steel is eight M13 bars (#4) equally spaced with a clear spacing of 76 mm. This section is shown in Figure 3.7, Section A-A.

Results for Case 1

The results for the columns modeled in OpenSees using hinge-Radau integration closely match the experimental results provided by Hewes and Priestly (2002). The comparison of the pushover analysis is shown in Figure 3.8. This figure compares the modeled results to the experimental results found by Hewes and Priestly (2002). For the first test, the OpenSees solution matches the elastic response of the column and the post yield response, but it slightly underestimates the stiffness at yield. For the second test, the OpenSees solution matches the elastic response and the inelastic response, but overestimates the stiffness at yield. This model does not accurately predict the ultimate strength and strain of the structure because the modeled

material properties do not have a defined failure strain. The analysis is stopped at 3% drift for test 1 and 6% drift for test 2 to correspond to failure during the experimental tests.

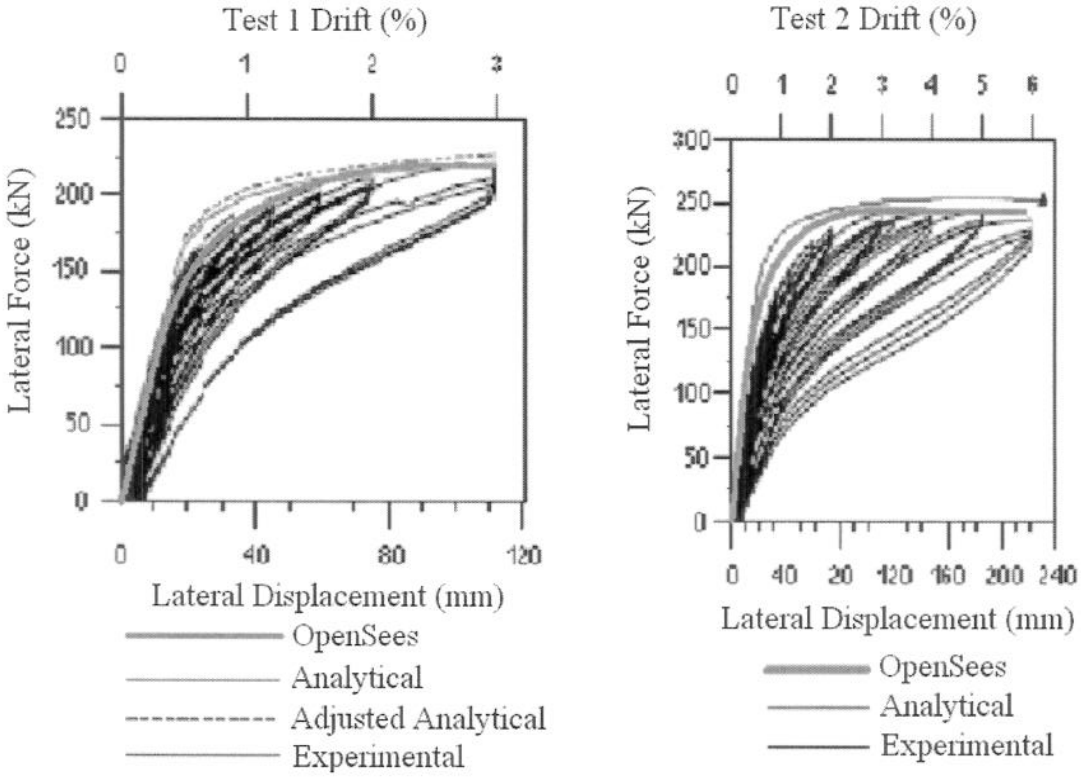

Figure 3.8: Results for test 1 and test 2 for case 1 of a lateral pushover analysis.

Case 2: Continuous Steel Jacket

The second case examined is the circular concrete column with a steel shell around the entire length. The data and design used to model this case come from Silva et al. (1999), which describes pushover analyses of three columns connected with a cap beam.

Geometry for Case 2

The geometry for case two is shown in Figure 3.9. Three CISS columns are connected at their tops by a concrete cap beam. The columns are 4.34 m tall and have a diameter of 910 mm. The steel jackets have a thickness of 12.70 mm. The columns have reinforcement ratios of 2.5% with (16) M36 bars (#11) symmetrically spaced in a diameter of 787 mm. The columns are spaced at 4.27 m center to center. Each column rests on a 610 mm tall concrete foundation, which is bolted to a strong floor. The cap beam is 1.07 m tall by 1.37 m wide and is designed to be rigid relative to the columns. The structure is loaded in the vertical direction before the pushover analysis starts. A continuous load is placed over each span between columns. The continuous load is equivalent to two point loads 1.2 m away from the center of the columns. The exterior point loads are 1223 kN and the interior point loads are 445 kN. The pin connection is used by Silva et al. (1999) to approximate half of a fixed-fixed column subject to lateral displacement at one end. This reduces the size of the experimental model.

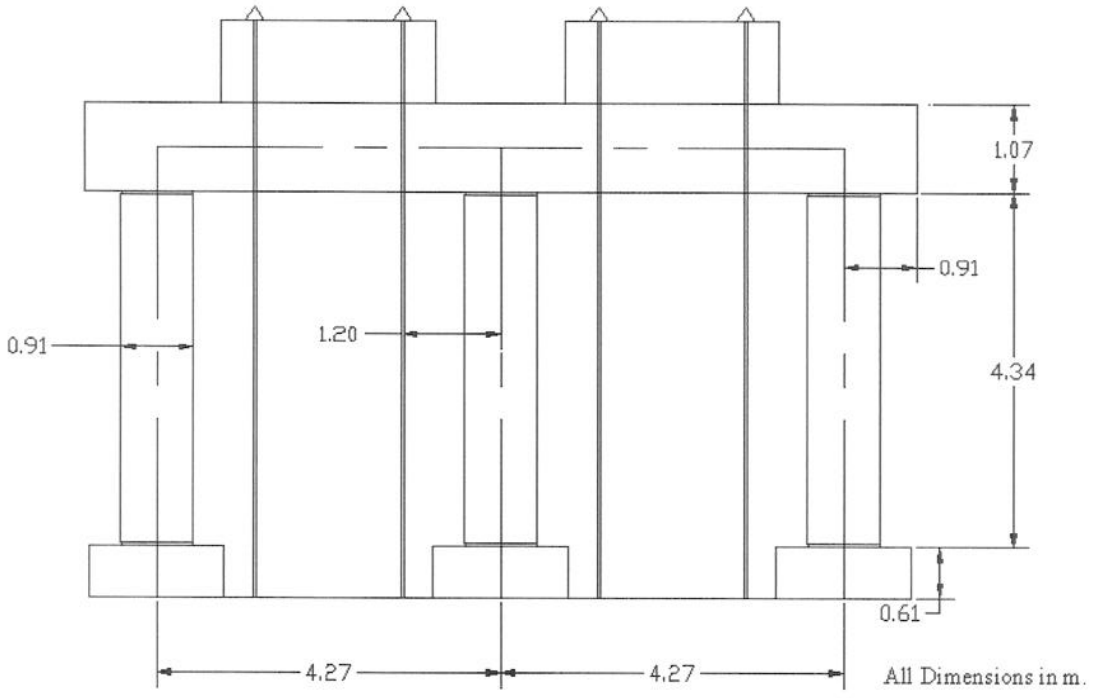

Figure 3.9: Geometry for case 2.

Modeling for Case 2

The three CISS columns and the cap beam are modeled in a two dimensional system with three degrees of freedom. The model consists of ten nodes and nine elements. The layout of the model is shown in Figure 3.10. The bottom node of each column is fixed in the X and the Y directions, but it is free to rotate in the Z direction to simulate the pin connection. One force-based beam-column element with modified hinge-Radau integration is used to model each column.

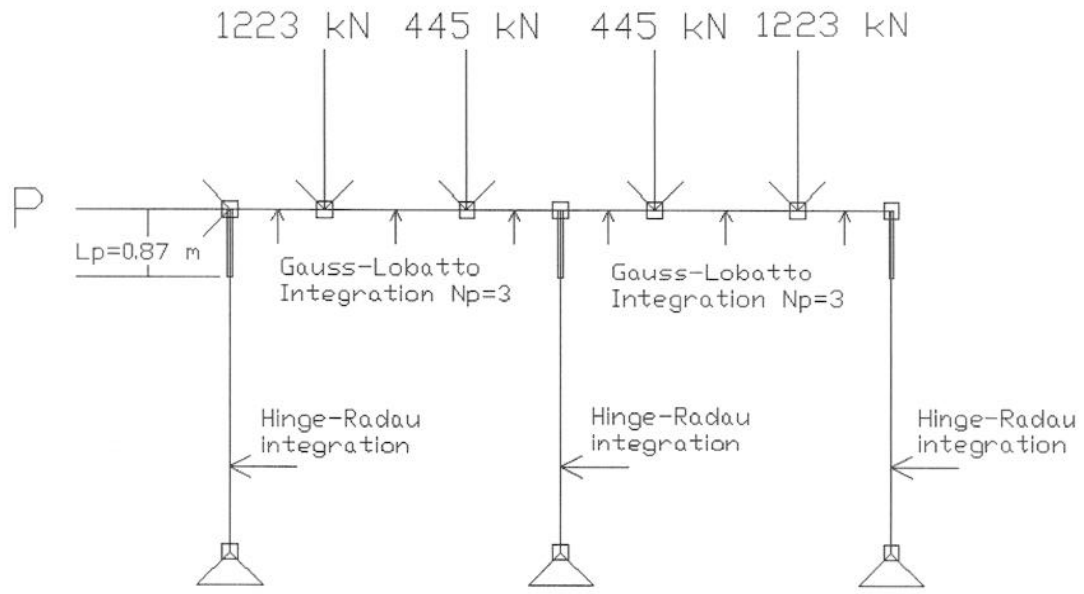

Figure 3.10: OpenSees model layout for Case 2.

A circular composite section combining the concrete, the reinforcing steel, and the steel jacket is used to model the columns. The concrete material has an unconfined strength, f'_c, of 35 MPa. The concrete has a confined strength of 86 MPa and is determined using the Mander model for confined concrete. The diameter of the concrete is 846 mm. The reinforcing steel has an elastic modulus of 200,000 MPa and a yield strength of 448 MPa with a strain hardening ratio of 2%. The reinforcing steel is equally spaced around the column with a clear spacing of 76 mm to the outside of the steel shell. The steel shell has a thickness of 12.7 mm, an elastic modulus of 200,000 MPa, yield strength of 250 MPa and a strain hardening ratio of 2%. Data for the strain hardening ratio is unavailable, so it is approximated from the results of the test.

The plastic hinge length is 868 mm and is located at the top of the column where it connects to the cap beam. The steel jacket flexural strength for the plastic hinge region is determined by taking an average of the steel jacket flexural strength over the bond transfer length determined by Chai et al. (1994). This approximation gives an average steel yield strength of 144 MPa for the plastic hinge region. In the elastic section the bond between the steel jacket and the concrete is fully developed, so the full strength of the steel shell is included. The composite circular section is shown in Figure 3.11.

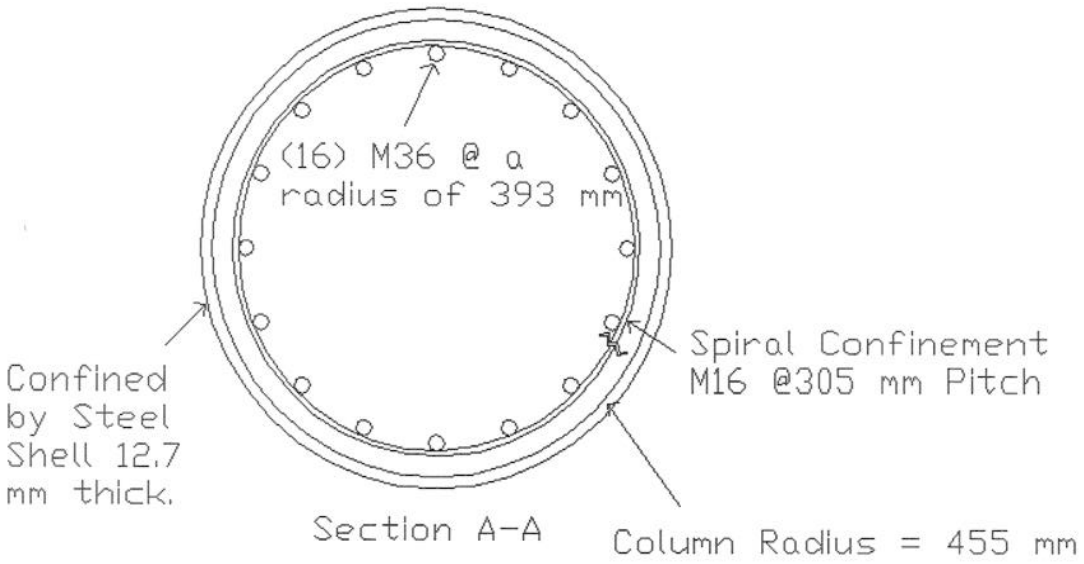

Figure 3.11: Composite circular column section for case 2.

The cap beam is modeled as a rigid member because its stiffness is significantly larger than that of the columns. To make a rigid cap beam the modulus of elasticity is increased to 200,000 MPa which is an order of magnitude stiffer than concrete. The cross-sectional area of the cap beam is 0.67 m^2. The cap beam consisted of three force-based beam-column elements with Gauss-Lobatto integration per span

with nodes at 1.2 m away from the center of each column. Three-point Gauss-Lobatto integration is used because the sections are uniform and expected to remain elastic. Vertical point loads are applied to each of the nodes in between the columns with 1,223 kN applied on the exterior nodes and 445 kN applied on the interior nodes to approximate the experimental loading. The simulated pushover analysis is conducted by the displacement control where the displacement of the center node on the cap beam is incrementally increased in the horizontal direction.

Results for Case 2

The results of the pushover analysis show the column yielding at 2000 kN with a displacement of 60 mm. After yield, the response flattens out and continues linearly until failure. These results are shown in Figure 3.12 and are compared to those from the experimental pushover analysis. The comparison shows that the OpenSees model accurately predicts the response of the columns. The elastic response closely matches the experimental results. The strength is slightly underestimated at yield. The post-yield behavior also matches the experimental results assuming the 2% strain hardening approximation was valid. This model does not accurately predict the ultimate strength and strain of the structure because the modeled material properties do not have a defined failure strain. The analysis is stopped at 8% drift corresponding to where the experimental model failed.

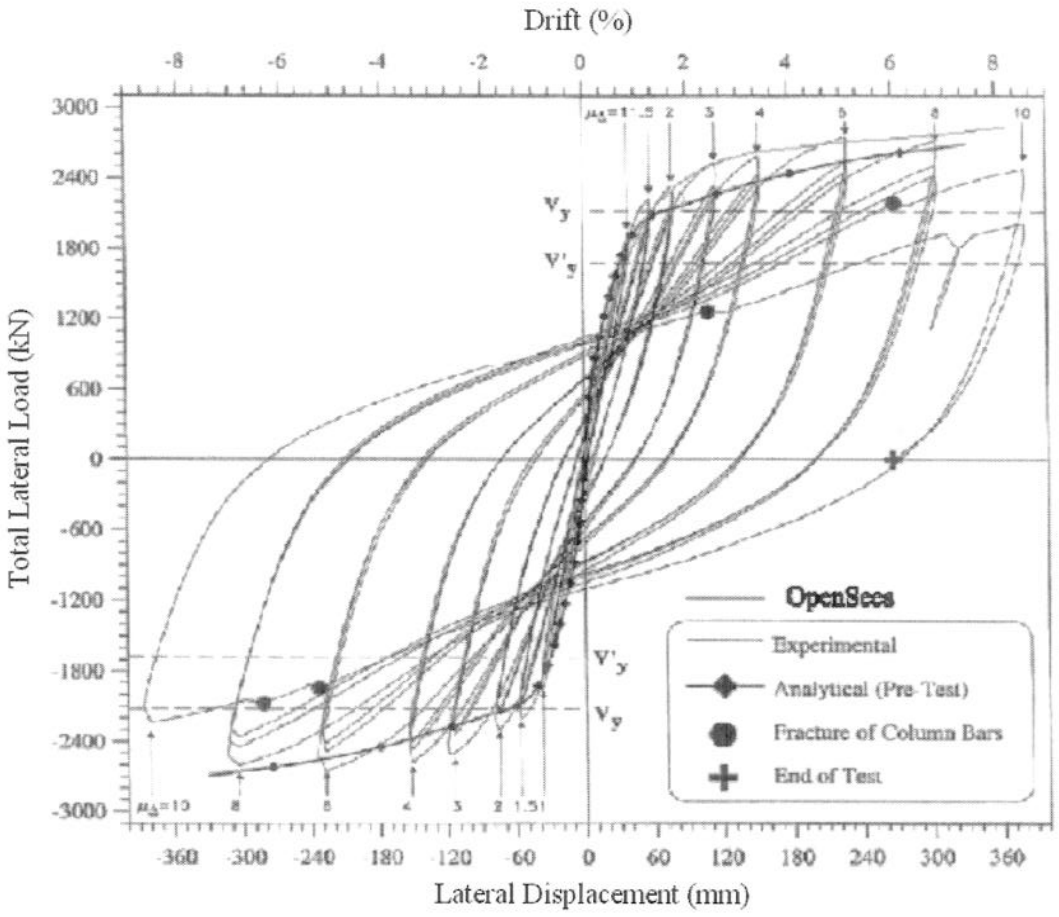

Figure 3.12: Comparison for case 2 of the experimental results and the modeled results.

Case 3: Continuous Steel Jacket in the Elastic Region

The third case considered is the circular concrete column with a steel shell around the elastic section. For this column type there is no experimental data available for comparison. Instead, the results are verified by hand calculations shown in Appendix B. This type of column is used to control the spread of the plastic hinge area and force the nonlinear behavior to occur in a specified area. This is done to control

the location of damage and facilitate repair after a seismic event. The geometry of this model is similar to the second case as it is taken from Silva et al. (1999).

Geometry for Case 3

The geometry for case three is shown in Figure 3.13. The three CISS columns are connected to the reinforced concrete cap beam along the top of each column. The columns are 4.34 m tall and have a diameter of 910 mm. The steel shells have a thickness of 12.7 mm. The columns have reinforcement ratios of 2.5% with (16) M36 bars (#11's) symmetrically spaced with a diameter of 787 mm. The columns are spaced at 4.27 m center to center. Each column sits on a 610 mm tall concrete foundation, which is bolted to a strong floor. The cap beam is 1.07 m tall by 1.37 m wide and is designed to be rigid relative to the columns. The structure is loaded in the vertical direction before the pushover analysis starts. The continuous load is equivalent to two point loads 1.2 m away from the center of the columns. The exterior point loads are 1223 kN and the interior point loads are 445 kN. The plastic hinge length is 700 mm which is the length of the section unconfined by the steel jacket.

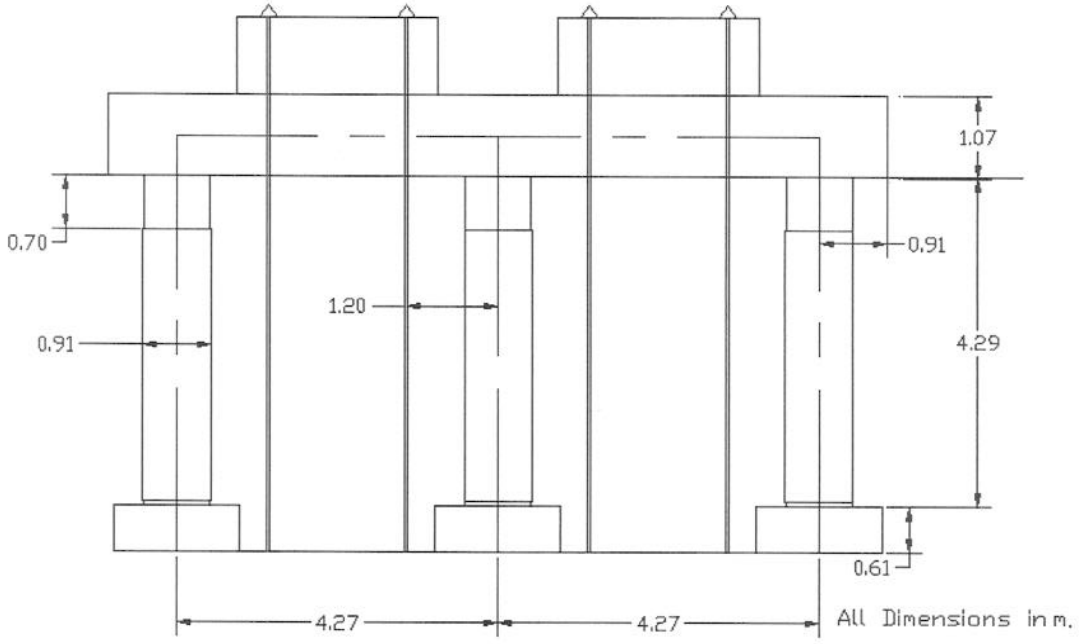

Figure 3.13: Geometry for case 3.

Modeling for Case 3

The columns are modeled using force-based beam-column elements with hinge-Radau integration. Two sections are used in the column elements. One is the reinforced concrete column with a steel jacket used in the elastic region of the column, and the other is a spiral confined concrete section used in the plastic hinge region. The plastic hinge region is at the end of the element connected to the cap beam.

The section used for the elastic region is the same as is used in case two. A circular composite section combining the concrete, the reinforcing steel, and the steel jacket is used to model the columns. The concrete material has a crushing strength, f'_c, of 35 MPa. The concrete has a confined strength of 86 MPa and is determined using the Mander model. The diameter of the concrete is 846 mm. The reinforcing steel has

an elastic modulus of 200,000 MPa and a yield strength of 448 MPa with a strain hardening ratio of 2%. The reinforcing steel is equally spaced around the column with a clear spacing of 76 mm to the outside of the steel shell. The steel shell has a thickness of 12.7 mm, an elastic modulus of 200,000 MPa, yield strength of 250 MPa and a strain hardening ratio of 2%.

The plastic hinge section consists of spirally confined concrete. The strength, f'_c, is 58 MPa at a strain of 0.003. The ultimate strength, f'_{cu}, is 44 MPa at an ultimate strain of 0.03. The model is shown in Figure 3.14. The reinforcing steel is the same as for the elastic section.

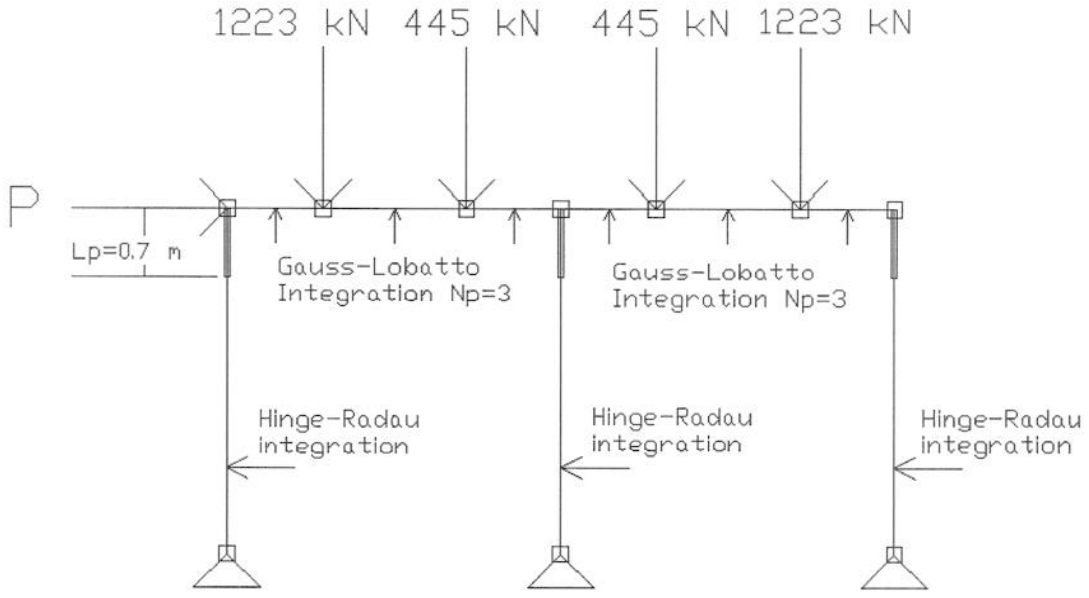

Figure 3.14: OpenSees model layout for case 3.

The cap beam is modeled as rigid, similar to case two, because its stiffness is significantly larger than that of the columns. To make a rigid cap beam the modulus of

elasticity is increased to 200,000 MPa and the area of the cap beam is 0.67 m^2 which is the same as in case two. The cap beam consisted of three force-based beam-column elements with Gauss-Lobatto integration per span with nodes at 1.2 m away from the center of each column. Three-point Gauss-Lobatto integration is used because the sections are uniform and expected to remain elastic. Point loads are applied to each of the nodes in the middle of the spans of 1,223 kN on the outside nodes and 445 kN on the inside nodes to approximate the experimental loading. The pushover analysis is conducted by displacement control where the displacement of the center node on the cap beam is incrementally increased in the horizontal direction.

Results for Case 3

The results of the pushover analysis are shown in Figure 3.15. The failure occurs in the plastic hinge region. The stiffness of the elastic portion of the column has minimal effect on the behavior after the plastic hinge region begins to yield. From hand calculations, it is shown that the nominal point load capacity of the spirally confined circular columns is about 1,585 kN (Nilson et al. 2004). The hand calculations are shown in Appendix B. This is close to the values predicted by the OpenSees model.

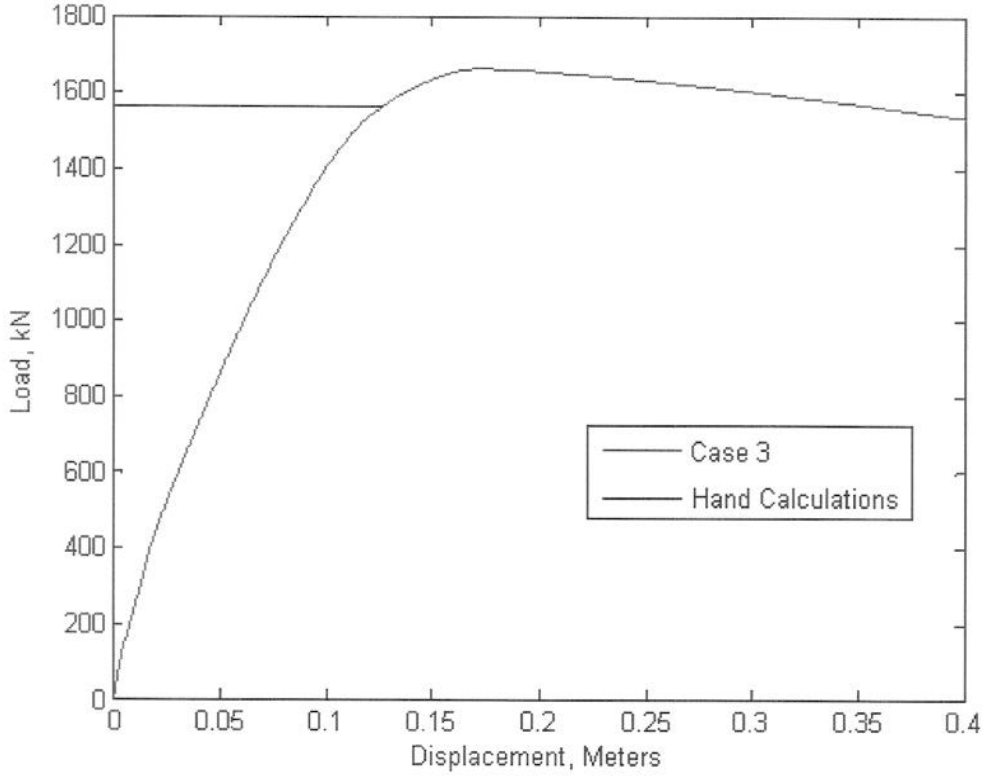

Figure 3.15: Modeled results for case 3 compared to the hand calculations.

Conclusion

This chapter presents an application of a plastic hinge integration method based on modified two-point Gauss-Radau quadrature to model circular concrete bridge columns with steel jackets. It is shown that using this integration method it is possible to obtain a simulated response which closely matches experimental data for two of the test cases and matches the hand calculations for the third case. From the results, it is shown that the hinge-Radau integration method can accurately and efficiently simulate the experimental response of reinforced concrete columns with steel jackets.

References

Chai, Y. H., Priestly, M. J. N., and Seible, F. (1991). "Seismic retrofit of circular bridge columns for enhanced flexural performance." *ACI Structural Journal*, 88(5), 572-584.

Chai, Y. H., Priestly, M. J. N., and Seible, F. (1994). "Analytical model for steel-jacketed RC circular bridge columns." *Journal of Structural Engineering*, 120(8), 2358-2376.

Hewes, J. T., Priestly, M.J.N. (2002) "Seismic design and performance of precast concrete segmental bridge columns." *Structural Systems Research Project, Report* No. SSRP-2001/25, University of California at San Diego, La Jolla, California.

Mander, J. B., Priestly, M. J. N., and Park, R., (1988) "Theoretical stress-strain model for confined concrete." *Journal of the Structural Division, ASCE*, 114(8), 1804-1826.

Neuenhofer, A., and Filippou, F. C. (1997). "Evaluation of nonlinear frame finite-element models." *Journal of Structural Engineering*, 123(7), 627-641.

Nilson, A. H., Darwin, D., and Dolan, C. W. (2004). *Design of Concrete Structures, 13th Edition*, McGraw-Hill, NewYork.

PCI Design and Handbook, Precast and Prestressed Concrete, 6th Edition, MNL-120-04, Prestressed/Precast Concrete Institute, Chicago, (2004).

Scott, M. H., and Fenves, G. L. (2006). "Plastic hinge integration methods for force-based beam–column elements." *Journal of Structural Engineering*, 132(2), 244-252.

Silva, P. F., Sritharan, S., Seible, F., and Priestly, M. J. N. (1999) "Full-scale test of the Alaska cast-in-place steel shell three column bridge bent." *Structural Systems Research Project*, Report No. SSRP 98/13, University of California at San Diego, La Jolla, California.

Chapter 4: Conclusions

The plastic hinge integration using modified two-point Gauss-Radau quadrature method (hinge-Radau) creates an accurate and computationally efficient numerical model for columns with different section properties in the plastic hinge region and the elastic region. The use of plastic hinge integration to model different section properties in the two regions is verified by comparing the response of a cantilever, using hinge-Radau integration, to the theoretical response of the same cantilever. The results show that hinge-Radau integration method closely approximates the nonlinear response of the cantilever. This result verifies that the hinge-Radau integration method can be used to model the behavior of structural systems with beam-columns that have plastic hinges. It also keeps the number of equations to a minimum because only one element is used for each frame member to make the solution method as efficient as possible.

The application of hinge-Radau integration to reinforced concrete columns with steel jackets is examined. Three cases are explored with the designs and the experimental responses provided by Hewes and Priestly (2002) and Silva et al. (1999). The comparison of the results validates that the hinge-Radau integration method can, accurately and efficiently, simulate the experimental response of steel-jacketed columns. It is recommended that the force-based beam-column with hinge-Radau integration be used for nonlinear analysis of reinforced concrete columns with steel jackets.

Bibliography

Chai, Y. H., Priestly, M. J. N., and Seible, F. (1991). "Seismic retrofit of circular bridge columns for enhanced flexural performance." *ACI Structural Journal*, 88(5), 572-584.

Chai, Y. H., Priestly, M. J. N., and Seible, F. (1994). "Analytical model for steel-jacketed RC circular bridge columns." *Journal of Structural Engineering*, 120(8), 2358-2376.

Coleman, J. and Spacone, E. (2001). "Localization issues in force-based frame elements." *Journal of Structural Engineering*, Vol. 127, No. 11, 1257-1265.

Hewes, J. T., Priestly, M.J.N. (2002) "Seismic design and performance of precast concrete segmental bridge columns." *Structural Systems Research Project, Report* No. SSRP-2001/25, University of California at San Diego, La Jolla, California.

Mander, J. B., Priestly, M. J. N., and Park, R., (1988) "Theoretical stress-strain model for confined concrete." *Journal of the Structural Division, ASCE*, 114(8), 1804-1826.

McKenna, F., Fenves, G. L., Scott, M. H., and Jeremic, B. (2000). "Open system for earthquake engineering simulation" <http://opensees.berkeley.edu>

Neuenhofer, A., and Filippou, F. C. (1997). "Evaluation of nonlinear frame finite-element models." *Journal of Structural Engineering*, 123(7), 627-641.

Neuenhofer, A., and Filippou, F. C. (1998). "Geometrically nonlinear flexibility-based frame finite element." *Journal of Structural Engineering*, 124(6), 704-711.

Nilson, A. H., Darwin, D., and Dolan, C. W. (2004). *Design of Concrete Structures, 13th Edition*, McGraw-Hill, NewYork.

PCI Design and Handbook, Precast and Prestressed Concrete, 6th Edition, MNL-120-04, Prestressed/Precast Concrete Institute, Chicago, (2004).

Scott, M. H., and Fenves, G. L. (2006). "Plastic hinge integration methods for force-based beam–column elements." *Journal of Structural Engineering*, 132(2), 244-252.

Silva, P. F., Sritharan, S., Seible, F., and Priestly, M. J. N. (1999) "Full-scale test of the Alaska cast-in-place steel shell three column bridge bent." *Structural Systems Research Project*, Report No. SSRP 98/13, University of California at San Diego, La Jolla, California.

Spacone, E., Ciampi,V., and Filippou, F. C. (1996). "Mixed formulation of nonlinear beam finite element." *Computers & Structures*, 58,71-83.

Appendices

Appendix A: Theoretical Solution for Cantilever

The following shows the calculations for the displacement of the cantilever beam. To calculate the displacement of the cantilever the principle of virtual forces is applied.

$U = \int_0^L m(x)\kappa(x)\,dx$ Where m(x) is the virtual moment and κ(x) is the curvature.

$m(x) = x$ for $0 < x < L$

and

$\kappa(x) =$

$\frac{P \cdot x}{E_1 I_1}$ for $0 < x < L - \beta L$

$\frac{P \cdot x}{E_2 I_2}$ for $L - \beta L < x < \zeta L$

$\frac{P_y \cdot x}{E_2 I_2}$ for $\zeta L < x < L$

$\frac{P \cdot x \cdot (\zeta - 1)}{\alpha \cdot E_2 I_2} + \frac{P \cdot x^2}{\alpha \cdot E_2 I_2 \cdot L}$. for $\zeta L < x < L$

where $\zeta = \max(0, 1 - My / M)$ and ζ describes the spread of plasticity across the plastic hinge length. The length ζL is the length of the cantilever over which m(x) is greater than M_y.

This gives:

$$U_1 = \int_0^{L-\beta\cdot L} \frac{P\cdot x^2}{E_1 I_1}\,dx$$

$$U_2 = \int_{L-\beta\cdot L}^{L-\zeta\cdot L} \frac{P\cdot x^2}{E_2 I_2}\,dx$$

$$U_3 = \int_{L-\zeta\cdot L}^{L} \frac{P_y\cdot x^2}{E_2 I_2}\,dx$$

$$U_4 = \int_{L-\zeta\cdot L}^{L} \frac{P\cdot x^2\cdot(\zeta-1)}{\alpha\cdot E_2 I_2} + \frac{P\cdot x^3}{\alpha\cdot E_2 I_2\cdot L}\,dx$$

Integrate to get:

$$U_1 = \frac{P\cdot(L-\beta\cdot L)^3}{3\cdot E_1 I_1}$$

$$U_2 = \frac{P\cdot\left[(L-\zeta\cdot L)^3-(L-\beta\cdot L)^3\right]}{3\cdot E_2\cdot I_2}$$

$$U_3 = M_y\left[\frac{L^3-(L-\zeta L)^3}{3\cdot E_2\cdot I_2}\right]$$

$$U_4 = \frac{P\cdot L^3\left[4L\cdot(\zeta-1)+3L\right]}{12\alpha\cdot E_2\cdot I_2\cdot L} - \frac{P\cdot(L-\zeta L)^3\left[4L\cdot(\zeta-1)+3(L-\zeta L)\right]}{12\alpha\cdot E_2\cdot I_2\cdot L}$$

U_4 simplifies to:

$$U_4 = \frac{P \cdot L^3 \left[(4\zeta - 1) + (1 - \zeta)^4 \right]}{12\alpha \cdot E_2 \cdot I_2}$$

For the elastic case where $P < P_y$, terms U_3 and U_4 become zero giving:

$$U_E = U_1 + U_2 = \frac{P \cdot (L - \beta \cdot L)^3}{3 \cdot E_1 I_1} + \frac{P \cdot \left[(L - \zeta \cdot L)^3 - (L - \beta \cdot L)^3 \right]}{3 \cdot E_2 \cdot I_2}$$

For the inelastic case where $P > P_y$:

$$U = U_1 + U_2 + U_3 + U_4$$

$$U = \frac{P \cdot (L - \beta \cdot L)^3}{3 \cdot E_1 I_1} + \frac{P \cdot \left[(L - \zeta \cdot L)^3 - (L - \beta \cdot L)^3 \right]}{3 \cdot E_2 \cdot I_2} + M_y \left[\frac{L^3 - (L - \zeta L)^3}{3 \cdot E_2 \cdot I_2} \right] + \frac{P \cdot L^3 \left[(4\zeta - 1) + (1 - \zeta)^4 \right]}{12\alpha \cdot E_2 \cdot I_2}$$

Appendix B: Hand Calculations for Load Capacity for Case 3

The flexural capacity of the concrete column from case three is computed as follows. The following equations control the behavior of the column. Figure B.1 shows the layout of the column section and the flexural resistance.

Variables:

Height = 4.34 m

f'_c = Compression Strength of Concrete

f_s = Steel Stress

E = Elastic Modulus of Steel

c = Distance to Neutral Axis

β_1 = Variable to Define the Depth of Stress Block

$a = \beta_1 c$

A_c = Area of Concrete Along Length a

ε_s = Steel Strain

ε_u = Concrete Strain = 0.003

d = Distance to Steel

C = Concrete Force

L_c = Length from Concrete Centroid to N.A.

T_i = Steel Force for Steel Bar i

L_i = Length from Steel i to N.A.

M_n = Nominal Moment Capacity for Section

P_n = Nominal Load Capacity = M_n/Height

Equations:

$$f_s = E\,\varepsilon_s$$

$$\varepsilon_s = \varepsilon_u \frac{d-c}{c}$$

$$C = 0.85\,f'_c\,A_c$$

$$T_i = A_s(f_s)_i$$

$$M_n = CL_c + \sum_i T_i L_i$$

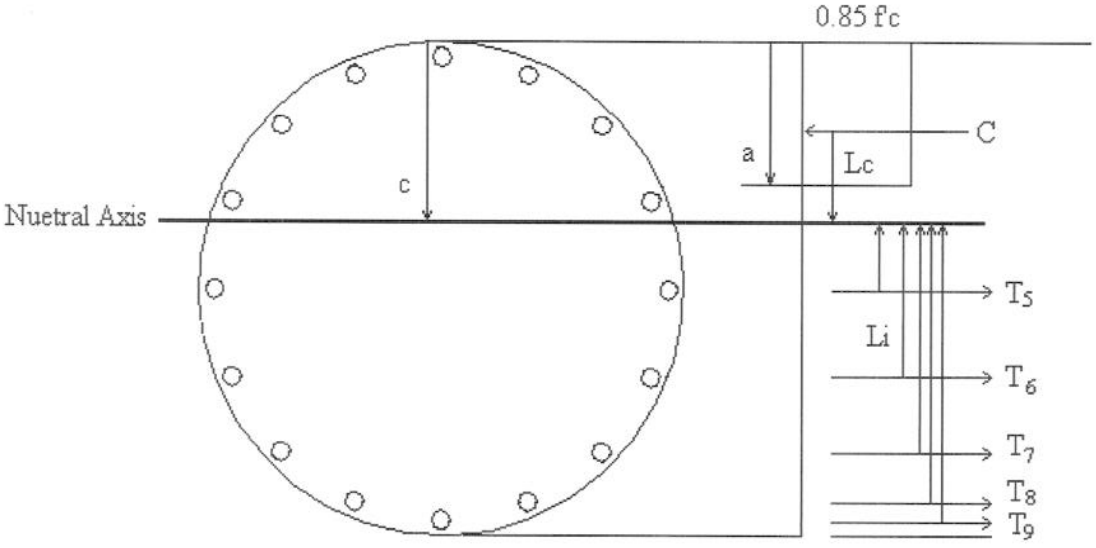

Figure B.1: Flexural resistance of the concrete section.

Excel was used to goal seek for the neutral axis. Equilibrium was found with c = 260 mm. The results are shown in Table B.1. The sum of all of the moments is 2293 kN m. To calculate the force, divide the moment by the moment arm of 4.34 m which gives 528 kN. To account for the three columns used in each bent the force is multiplied by three to give a calculated force of 1585 kN.

Table B.1: Calculations for Flexure in a Reinforced Concrete Section

Concrete Properties		c (mm)		a (mm)		y1(mm)		concrete area (m2)		
		259		168		225		0.076		
Steel Area		As1	As2	As3	As4	As5	As6	As7	As8	As9
(mm)		1006	2012	2012	2012	2012	2012	2012	2012	1006
Steel Strain		et1	et2	et3	et4	et5	et6	et7	et8	et9
		-0.003	-0.003	-0.002	-2E-04	0.0016	0.0033	0.0048	0.0058	0.0061
Steel Stress		fs1	fs2	fs3	fs4	fs5	fs6	fs7	fs8	fs9
		0	0	0	0	413	413	413	413	413
Forces	Concrete	As1Fs1	As2fs2	As3Fs3	As4Fs4	As5Fs5	As6Fs6	As7Fs7	As8Fs8	As9Fs9
(kN)	-3744	0	0	0	0	832	832	832	832	416
Moment Arm	Concrete	c1	c2	c3	c4	c5	c6	c7	c8	c9
(mm)	-259	-259	-229	-144	-16	134	285	412	497	527
Moment	Mc	M1	M2	M3	M4	M5	M6	M7	M8	M9
kNm	969	0	0	0	0	112	237	343	414	219